UNIVERSITY OF SÃO PAULO
SÃO CARLOS SCHOOL OF ENGINEERING

Leonardo Ferreira dos Santos

PHYSICAL CONGRUENCE OF COMPUTATIONAL MODEL AND OPTIMIZATION OF JET ENGINE MODEL IN COMPUTATIONAL FLUID DYNAMICS

São Carlos

2025

Leonardo Ferreira dos Santos

PHYSICAL CONGRUENCE OF COMPUTATIONAL MODEL AND OPTIMIZATION OF JET ENGINE MODEL IN COMPUTATIONAL FLUID DYNAMICS

Thesis presented to the Aeronautical Engineering undergraduate program at the São Carlos School of Engineering, University of São Paulo, as part of the requirements to obtain the degree of Aeronautical Engineer. .

Advisor: Paulo Celso Greco Júnior, Ph.D.

São Carlos

2025

Ficha catalográfica elaborada pela Biblioteca Prof. Dr. Sérgio Rodrigues Fontes da EESC/USP com os dados inseridos pelo(a) autor(a).

Ferreira dos Santos, Leonardo
F237p PHYSICAL CONGRUENCE OF COMPUTATIONAL MODEL AND OPTIMIZATION OF JET ENGINE MODEL IN COMPUTATIONAL FLUID DYNAMICS / Leonardo Ferreira dos Santos; orientador Paul Celso Greco Júnior. São Carlos, 2025.

Monografia (Graduação em Engenharia Aeronáutica) -- Escola de Engenharia de São Carlos da Universidade de São Paulo, 2025.

1. CFD. 2. Engine efficiency. 3. Jet turbine. 4. Computational simulation. 5. Specific Fuel Consumption. I. Título.

Eduardo Graziosi Silva - CRB - 8/8907

FOLHA DE APROVAÇÃO
Approval sheet

Candidato / *Student*: Leonardo Ferreira dos Santos
Título do TCC / *Title* : PHYSICAL CONGRUENCE OF COMPUTATIONAL MODEL AND OPTIMIZATION OF JET ENGINE MODEL IN COMPUTATIONAL FLUID DYNAMICS
Data de defesa / *Date*: 07/07/2025

Comissão Julgadora / *Examining committee*	**Resultado** / *result*
Professor Associado Paulo Celso Greco Jr	APROVADO
Instituição / Affiliation: EESC - SAA	
Professor Associado Hernan Dario Ceron Muñoz	APROVADO
Instituição / Affiliation: EESC - SAA	
Professor Doutor Álvaro Martins Abdalla	APROVADO
Instituição / Affiliation: EESC - SAA	

Presidente da Banca / Chair of the Examining Committee:

Professor Associado Paulo Celso Greco Jr
(assinatura / *signature*)

For those who never knew where the ground was — and so chose to fly.

ACKNOWLEDGEMENTS

The completion of this study was only possible thanks to the dedication and support of several people who, in one way or another, played an important role in my development, both academically and personally. Therefore, I would like to express my sincere gratitude to each one who supported me throughout this journey.

First of all, I express my gratitude to God for the energy and discernment that allowed me to complete this stage, as well as for the opportunity to walk this path I am now concluding.

To my family, especially my mother Meire, my father Claudinei, my brother Gabriel, and my girlfriend Maria Eduarda, for their boundless affection, constant support, strength, love, care, words of encouragement, and for the patience shown at all times—whether in moments of difficulty or success. On the darkest and coldest days, you were certainly the light and warmth in my life, guiding me and helping me become who I want to be in the future and who I am today. Without you, I certainly wouldn't be where I am, and I will be forever grateful to each of you. For that, I leave here my heartfelt thanks and the certainty that I will continue to count on you, wherever I may be, wherever I go—you will always be with me in my heart and mind.

To my advisor, Professor Dr. Paulo Celso Greco Jr., for his precise guidance, openness to help, and encouragement throughout the development of this work. His ideas and knowledge were fundamental to the progress of this research.

To the professors of the Aeronautical Engineering program, who shared their knowledge and encouraged my intellectual, professional, and personal growth.

To my classmates and friends—especially Fernando, Pedro, Murilo, Paulo, Gustavo, Saulo, Jhonny, Thiago, Caio, Matheus, Guilherme, Victor, João Paulo, Kyara, Ana Paula, Sofia, Pablo, João Pedro, Enzo, Mariana, and so many others—for their camaraderie, shared experiences, and light-hearted moments that made this journey more pleasant, easier, and truly unforgettable.

To the organizations and professionals who assisted in this research by providing information or any other form of technical support.

Finally, to everyone who, in some way, contributed to the realization of this work and to my learning, my most sincere and heartfelt thanks.

São Carlos, 2025

Leonardo Ferreira dos Santos

“O sucesso é ir de fracasso em fracasso sem perder o entusiasmo”

ABSTRACT

SANTOS, L. F. d. **Physical congruence of computational model and optimization of jet engine model in Computational Fluid Dynamics**. 2025. 85 p. Monograph (Conclusion Course Paper) - São Carlos School of Engineering, University of São Paulo, São Carlos, 2025.

This work aims to validate the physical consistency of a three-dimensional computational model of a jet engine using CFD (Computational Fluid Dynamics), as well as to explore strategies for improving its efficiency. Initially, a significant physical inconsistency was observed between the torques of the turbine and compressor, prompting adjustments such as varying engine speed and fuel injection rate. Once congruence was achieved, optimization strategies were implemented, including adjustments to the turbine blade angle of attack and resizing of the combustion chamber injectors. Using the Merlin 90 jet engine as an experimental basis, results showed that even with computational and modeling limitations, the modifications applied led to meaningful improvements in thrust and specific fuel consumption. Therefore, the computational approach proved to be a cost-effective and technically viable method for preliminary studies in aircraft propulsion.

Keywords: CFD. Engine efficiency. Specific Fuel Consumption. Jet turbine. Computational simulatio

RESUMO

SANTOS, L. F. d. **Congruência física de modelo computacional e otimização de modelo motor a jato em Computional Fluid Dynamics**. 2025. 85 p. Monografia (Trabalho de Conclusão de Curso) - Escola de Engenharia de São Carlos, Universidade de São Paulo, São Carlos, 2025.

O presente trabalho tem como objetivo validar a coerência física de um modelo computacional tridimensional de motor a jato em CFD (Computational Fluid Dynamics), além de explorar formas de otimização da eficiência do modelo. Inicialmente, identificou-se uma incongruência física significativa nos torques entre turbina e compressor, o que motivou a investigação de ajustes no modelo, como a variação da rotação e da taxa de injeção de combustível. A partir da correção da incongruência, foram aplicadas estratégias de aumento de eficiência, como a otimização da geometria das pás da turbina (ângulo de ataque) e o redimensionamento dos injetores da câmara de combustão. Utilizando o motor real Merlin 90 como base experimental, os resultados mostraram que mesmo com limitações computacionais e simplificações adotadas, as modificações aplicadas no modelo geraram ganhos relevantes em empuxo e consumo específico de combustível. A abordagem computacional, portanto, demonstrou-se como uma alternativa economicamente viável e tecnicamente eficaz para estudos preliminares de propulsão aeronáutica.

Palavras-chave: CFD. Eficiência de motor. Consumo específico de combustível. Turbina a jato. Simulação computacional.

LIST OF FIGURES

LIST OF TABLES

LIST OF ABBREVIATIONS AND ACRONYMS

USP	University of São Paulo
USPSC	USP São Carlos Campus
CFD	*Computational Fluid Dynamics*
CAD	*Computer-Aided Design*
CAE	*Computer-Aided Engineering*
ECU	*Electronic Control Unit*
SAF	*Sustainable Aviation Fuel*
RANS	*Reynolds Averaged Navier-Stokes*
k–ε	*Turbulence model: kinetic energy–dissipation rate*

LIST OF SYMBOLS

List of Symbols

γ	Ratio of specific heats (adiabatic index)
T, T_0	Temperature / Stagnation temperature [K]
P, P_0	Pressure / Stagnation pressure [Pa]
ρ	Density [kg/m³]
U	Blade tangential speed [m/s]
c	Absolute velocity of fluid flow [m/s]
w	Relative velocity (rotating frame) [m/s]
α	Absolute flow angle [degrees]
β	Relative flow angle [degrees]
η	Efficiency (subscripts: c=compressor, t=turbine, b=combustion)
τ	Torque [N·m]
$\dot{m}$	Mass flow rate [kg/s] (subscripts: a=air, f=fuel)
M	Mach number
Re	Reynolds number
SFC	Specific Fuel Consumption [kg/N·s]
$\mathcal{T}$	Thrust [N]
Q_{comb}	Lower heating value of fuel [J/kg]
k	Turbulent kinetic energy [m²/s²]
ε	Turbulent dissipation rate [m²/s³]
R	Specific gas constant [J/kg·K]
A	Cross-sectional area [m²]
r	Radial coordinate [m]
f	Fuel-to-air ratio ($\dot{m}_f/\dot{m}_a$)
h_0	Stagnation enthalpy [J/kg]
a	Speed of sound [m/s]
C_p	Specific heat at constant pressure [J/kg·K]

CONTENTS

1 INTRODUCTION

Environmental awareness around the world has evolved considerably in recent years across various sectors. This has led modern industry to adopt business models that asymptotically pursue the utopia of sustainable development, which, in pragmatic terms, is reflected as growth with minimal environmental damage, according to criteria established by official environmental organizations worldwide.

Aviation is certainly one of the sectors with significant responsibility for pollutant gas emissions, accounting for 2.5% of global carbon dioxide (CO_2) emissions, one of the main greenhouse gases (AGÊNCIA INTERNACIONAL DE ENERGIA, 2025).

Seeking to increase environmental responsibility and mitigate the effects of its operations, multiple companies in modern aviation have adhered to the agreement established through a joint effort by the *International Civil Aviation Organization* (ICAO) and the United Nations, known as the *Carbon Offsetting and Reduction Scheme for International Aviation* (CORSIA). The agreement is structured in three phases, the last of which is mandatory, and aims to reduce greenhouse gas emissions from international flight operations by 2030 (ORGANIZAÇÃO DA AVIAÇÃO CIVIL INTERNACIONAL, 2025).

Additionally, some companies in the sector, such as EMBRAER, have published in their ESG (*Environmental, Social and Governance*) plans a commitment to achieving net-zero emissions by 2050, further expanding the scope of what is addressed in CORSIA.

The challenge of reducing pollutant gas emissions in the aviation sector is intrinsically linked to various efficiencies associated with the adopted business model. Specifically regarding the product, there are several ways to make an aircraft more efficient—meaning, capable of operating with lower fuel consumption. In 2024, fuel consumption represented approximately 32% of the operational costs for airlines (MERCADO & EVENTOS, 2024).

Primary approaches include increasing aerodynamic efficiency, reducing component weight, improving engine efficiency, and exploring more innovative alternatives such as the use of alternative fuels. These include Sustainable Aviation Fuel (SAF), hydrogen (H_2), and electric energy, all of which are applicable to aircraft development projects in the future.

Focusing on aircraft propulsion and a deeper analysis of engine efficiency optimization, many aircraft have achieved significant reductions in fuel consumption through improvements to their turbines, as shown over the decades in Figure 1.

A major Brazilian project worth mentioning in terms of improving engine efficiency was achieved by Embraer's Ejets family — the E2 190 compared to the older E1 generation, both shown respectively in Figure 2. The E2 190 achieved an 11% reduction in fuel consumption

Figure 1 – Fuel Efficiency Gain per Decade.

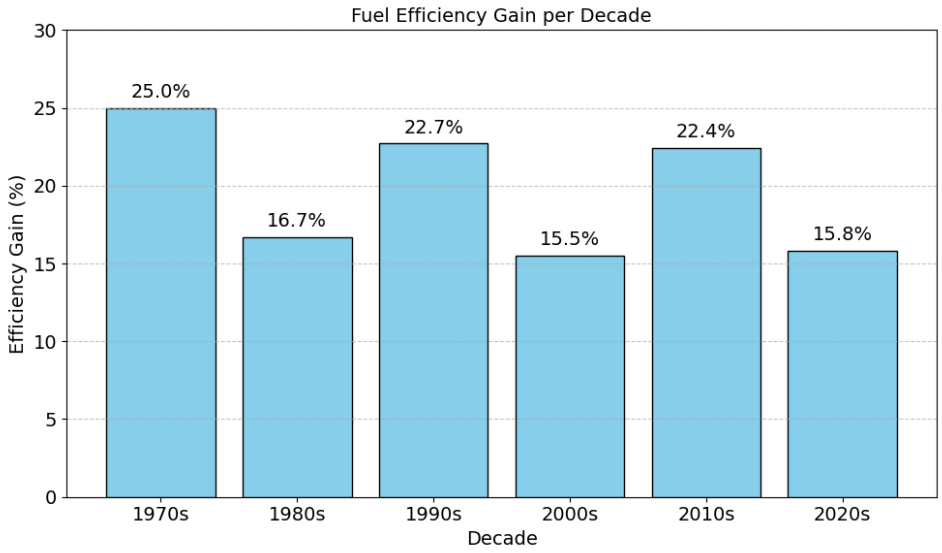

Source: Estimated based on data from ICAO, IEA, Boeing, Airbus, and open-access studies on aircraft fuel economy evolution (1960–2020).

through the use of the Pratt & Whitney PW1900G geared turbofan engine (AVIATION WEEK, 2025).

Figure 2 – E2-190 and E1 - 190

Test flight results confirm the Embraer E190-E2 as the most fuel-efficient single-aisle aircraft. Source: AeroMorning (2018).

Embraer E190 aircraft. Source: AeroMorning (2018).

With the aim of exploring this knowledge, which is not widely disseminated and is generally treated as a trade secret, the present work focuses on the use of simulation in *CFD* (*Computational Fluid Dynamics*), a much more cost-effective tool compared to wind tunnel testing, which is often unfeasible, without significant loss of fidelity, as a means to optimize and improve aircraft engines.

CFD is an engineering field that uses numerical methods to solve and analyze fluid flow problems. Due to the complexity of turbulent flows and the high computational demand required for their direct simulation, modeling techniques are employed to make the problem manageable.

One of the most commonly used approaches is the RAMS method (*Reynolds Averaged Modeling System*), better known as RANS (*Reynolds Averaged Navier-Stokes*).

The RAMS/RANS model consists of decomposing flow variables, such as velocity and pressure, into mean and fluctuating components. By applying this decomposition to the Navier-Stokes equations, the Reynolds-averaged Navier-Stokes equations are obtained, which describe the average behavior of the fluid over time. However, this averaging introduces additional terms, known as Reynolds stresses, which represent the effects of turbulence and need to be modeled to close the system of equations.

Furthermore, the work will explore the appearance and solutions to physical incompatibilities that may arise in the computational environment when simulating real phenomena, which must be addressed first in order for the CFD simulation to be valid.

For the study, the Merlin 90 model is used as a basis—a small gas turbojet engine for model aircraft, manufactured by the Spanish company Jets Munt S.L., which is illustrated in Figure 3.

Figure 3 – Turbojato Merlin 90

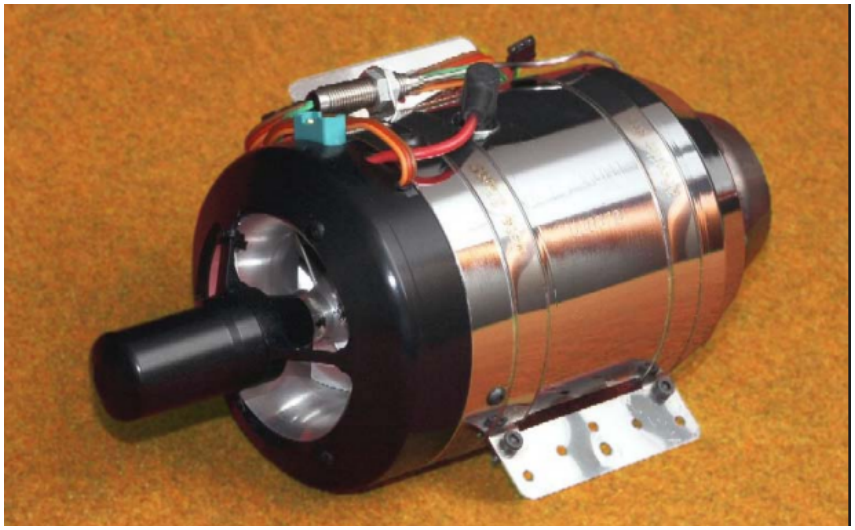

Jets Munt SL. Merlin 90/100/140/160 Instruction Manual, Version 3.1/2011, p. 8. Available on: jets-munt.com

The choice is mainly justified by the difficulty in obtaining geometries of larger engines and by the university's possession of the model, which facilitates the computational modeling of a turbojet engine. This model will be explored in the following chapters, as it is sufficient to reproduce theories and practices related to improving the efficiency of a general aviation engine.

2 PROBLEM DESCRIPTION

The present study begins with a problem of computational physical incongruence and progresses to a systematic dynamic optimization using both theoretical and empirical models of a computational dynamic model of a model aircraft jet turbine. The initial problem arose from a discrepancy between the torques generated by the turbine and the compressor, which showed a significant difference in value. Even considering the hypothesis of mechanical losses due to other elements, lubrication loss (since it is a real turbine), the behavior still appeared absurd, as these two elements are connected on the same shaft and therefore should exhibit very similar torque values.

The initial problem suggested in this research starts with a computational simulation discrepancy of approximately 47.2% between the turbine and compressor torques, with a nominal difference of 0.6273 $N \cdot m$, which is relatively high and not justified by mechanical losses or fluid energy losses, indicating a physical inconsistency in the model. At first, the research focused on finding solutions to mitigate or resolve this divergence—that is, to achieve power balance between the two components. The main approaches considered are:

- Adjusting the rotation until power equilibrium between turbine and compressor is reached
- Adjusting the amount of fuel injection in the combustion chamber until agreement between the torques of the two components is achieved

Building on the opportunity presented by the study, the second phase prioritized the analysis of improving the computational model's efficiency, which, in a very pragmatic way, is quite interesting and one of the main challenges in aerodynamics in general. It is also highly desirable in a real engine project or other elements of an aeronautical design, since small efficiency gains generate significant operational cost savings.

3 COMPUTIONAL MODEL

The construction of the aerodynamic model used in this study will be outlined in the following sections, presenting the sequence of actions taken prior to the numerical resolution of the simulation itself. It is important to highlight that the preprocessing stage of the computational aerodynamic model is one of the most critical steps of the simulation, as it is crucial to prepare the entire environment necessary to produce a numerical simulation that is correct, stable, and realistic. Incongruences will generate invalid results, inconsistent with reality, and may even prevent calculations altogether, causing various errors in the software involved.

3.1 Computer Aided Design

It is worth noting that the manufacturer Jets Munt S.L. does not possess CAD models, only technical drawings on paper, which, due to commercial confidentiality, were not shared with the University. For this reason, an approximate CAD model was developed for this study using the CATIA software, based on the real engine, since the Department of Aeronautical Engineering owns a Merlin 90 turbojet engine, to conceptualize the pertinent modifications. The base was a 3D CAD model obtained from the Internet, similar to the Jets Munt engine.

By disassembling the engine parts, it was possible to obtain a reasonable idea of the design of various components of the engine, except for the combustion chamber, which was not fully disassembled. For this, more conventional designs and similar engines were used as a reference. Figures 4 to 5 illustrate the conceptualization process of the turbine and compressor of the engine, the two main components of a turbojet, in CAD, since they represent parts of the disassembled engine.

Figure 4 – Compressor disassembled

Source: Doctor Professor Paulo Greco

Figure 5 – Turbine disassembled

Source: Doctor Professor Paulo Greco

It is appropriate to mention here that, due to the unavailability of the drawings, the aerodynamic profiles of the turbine blades and compressor blades were also conceptualized, with the premise of adjusting the flow leaving the stators at the airfoil leading edge and an attempt to reduce the rotational velocity of the flow to zero at the trailing edge, both at the blade root and tip. With these two profiles drawn, an extrapolation along the mean line was performed to obtain the final blade shape, for both the compressor and the turbine, which can be seen in Figures 6 to 7.

Figure 6 – Compressor Airfoil

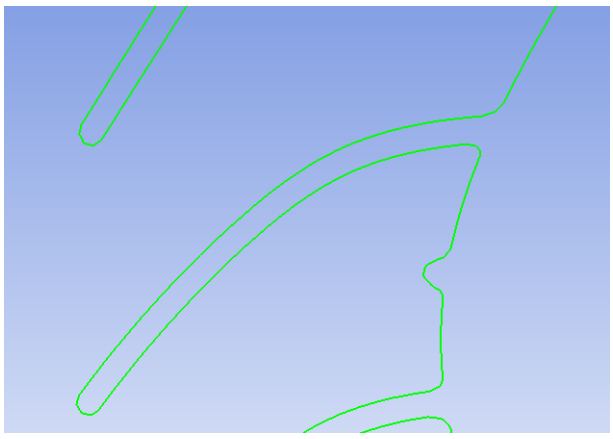

Source: Developed by the author

Figure 7 – Turbine Airfoil

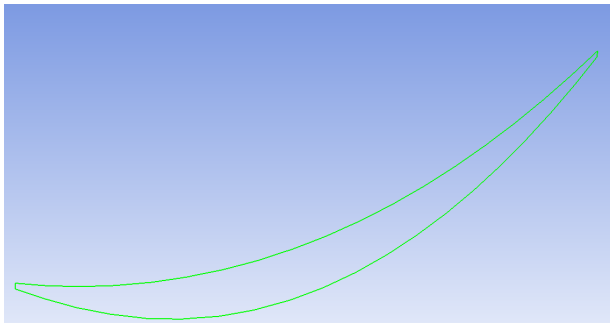

Source: Developed by the author

With these considerations, the CAD model illustrated in Figures 8 to 10 was obtained, allowing the construction of the CAE models that will be used for mesh modeling, which will be explored in the next section.

Figure 8 – Inlet, Intake and Compressor

Source: Developed by the author

Figure 9 – Compressor and Diffuser

Source: Developed by the author

Figure 10 – Chamber and Vanes

Source: Developed by the author

Figure 11 – Turbine and Nozzle

Source: Developed by the author

3.2 Mesh Generator

With the models illustrated in Figures 8 to 11, files were exported in the *.igs* format to import the geometries constructed in CAD into the mesh generator. In this study, the *ICEM CFD* tool, developed by *Ansys*, was used.

Generating components separately in CAD is justified at this stage, considering that components are also generated separately during meshing, as it optimizes mesh construction due to:

- **Cell deformation and distortion:** The entire assembly is much more complex than a single component, causing difficulties for the software to smooth the mesh, especially at contact points, resulting in irregular mesh elements.

- **Local refinement control:** Computational processing gains by allowing mesh refinement in critical elements and coarser meshes in less critical areas.

- **Interface intersection problems:** Conditions of overlap or gaps may be generated, which might not be detected in the full assembly due to its size.

- **Error diagnosis:** It is not necessary to redo the entire mesh, only the component presenting the error, and the identification of the problematic component is immediate, preventing simulation compromise.

Additionally, this approach allows the model to simulate components with relative motion between each other, such as the turbine and compressor, with greater stability.

Proceeding to the mesh, its creation process is quite straightforward and includes essential tools for identifying possible errors. With the geometry imported into *ICEM CFD*, geometric inconsistencies are checked and repaired—initially automatically by the software and later manually by deleting or adding geometric elements to make the model consistent. This can be visually identified through a color code.

With the geometry properly adjusted, the chosen approach was to generate the surface mesh initially, followed by local refinement in the most critical elements, and then generate the volumetric mesh elements.

In summary, the parameters used for mesh generation are shown in Table 1.

Table 1 – Global Mesh parameters

Component	Maximum Scale Factor	Maximum size of element [mm]
Inlet	1	2
Compressor	1	2
Difuser	1	2
Chamber	1	3
Vanes	1	0.75
Turbine	1	0.75
Nozzle	1	2

For the combustion chamber element, a refinement of 0.25 mm was applied to the injectors. All surface elements were generated using the *All Tri* method—triangular elements that adhere well to irregular and complex surfaces—and the volumetric (fluid) mesh was generated using the *Robust (Octree) Quick* method—hexahedral elements for simple geometries that perform well around geometric discontinuities, such as holes and intersections.

In this way, the meshes shown in Figures 12 to 14 were obtained.

Figure 12 – Mesh of Inlet and Compressor

Source: Developed by the author

Figure 13 – Mesh of Difuser and Chamber

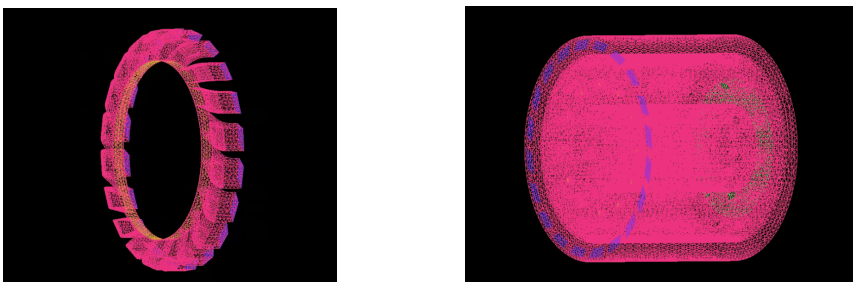

Source: Developed by the author

Figure 14 – Mesh of Vanes, Turbine and Nozzle

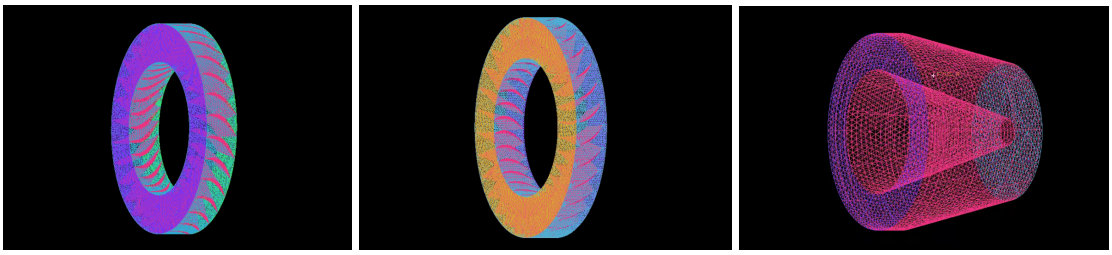

Source: Developed by the author

Having obtained the components separately, the final mesh can then be seen in Figure 15.

Figure 15 – Mesh of the complete engine

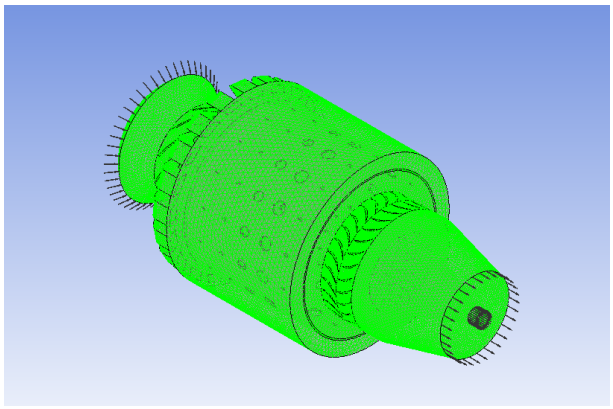

Source: Developed by the author

It is of utmost importance to highlight that due to the limitation imposed by the number of mesh nodes (512 thousand) allowed by the educational license used, combined with the high complexity of the model to be simulated (relative rotation between components, combustion chamber explosion generating high turbulence in the flow, fluid compression and expansion phases, complex geometry), the study was prevented from using a finer mesh refinement. Consequently, the mesh constructed can be classified as somewhat coarse but still maintains a reasonably good correlation with the expected behavior of a turbojet engine.

4 SIMULATION

4.1 Reynolds and Mach Number

In ANSYS CFX, when simulating turbo machinery such as turbojet engines, the Reynolds number is calculated automatically based on the inlet conditions and the characteristic dimensions of the flow region. The calculation is typically performed using the **rotor tip speed** as the characteristic velocity and the **rotor outer diameter** as the characteristic length. .

$$Re_{\text{turbojet}} = \frac{\rho_{\text{in}} \cdot (\omega R) \cdot D}{\mu_{\text{in}}} \tag{4.1}$$

Where:

- ω: rotor angular velocity ($\mathrm{rad/s}$),
- R: rotor radius (m),
- D: hydraulic diameter or reference length (m),
- Properties referenced at the domain inlet (boundary condition).

The Mach number (M) is a fundamental parameter in the analysis of compressible flows in turbomachinery, as it defines the ratio between the local flow velocity and the speed of sound. In *ANSYS CFX*, this number is calculated locally, based on the classical definition:

$$M = \frac{|\vec{V}|}{a} \tag{4.2}$$

where $|\vec{V}|$ represents the magnitude of the fluid velocity, and a is the local speed of sound, determined by:

$$a = \sqrt{\gamma \cdot R \cdot T} \tag{4.3}$$

where:

- γ: ratio of specific heats (1.4 for air);
- R: gas constant (287.05 J/kg·K for air);
- T: local flow temperature (in Kelvin).

In the context of turbomachinery, *CFX* differentiates the calculation of M according to the domain's frame of reference:

- **Stationary domains (stator):** the Mach number is calculated based on the **absolute velocity**, that is, the fluid velocity relative to a fixed reference frame.
- **Rotating domains (rotor):** the Mach number is calculated based on the **relative velocity**, i.e., the fluid velocity relative to the moving rotor.

The velocity relative to the rotor ($\vec{V}_{\text{rel}}$) is given by:

$$\vec{V}_{\text{rel}} = \vec{V}_{\text{abs}} - (\vec{\omega} \times \vec{r}) \tag{4.4}$$

where:

- $\vec{V}_{\text{abs}}$: absolute flow velocity;
- $\vec{\omega}$: angular velocity vector of the rotating domain;
- $\vec{r}$: position vector relative to the axis of rotation.

This distinction is crucial for correctly predicting subsonic, transonic, or supersonic flow regions within the machine. In rotor regions, using the relative velocity allows an accurate assessment of the severity of pressure gradients and shocks on the rotating blades.

In post-processing with *CFX-Post*, the Mach number can be accessed directly through the variable **Mach Number**, which automatically respects the local frame of reference of the domain, facilitating performance evaluation and phenomena such as shock waves or stall.

For the model, based on these equations, the values shown in Table 2 were obtained:

Table 2 – Mach and Reynolds Number

Reynolds Number	$3.4495 \cdot 10^5$
Mach Number	0.579

4.2 Pre-processing conditions for the simulation

After mesh construction, several parameters and conditions must be defined to ensure greater fidelity. At this stage of the study, considerations are made regarding the physical condition of the flow, fluid properties, boundary conditions for each face of the geometries, turbulence model, and initial conditions.

Although the problem is unsteady, to reduce the already high computational cost, a steady-state simulation was used. Nevertheless, the simulation begins with a transient regime until reaching what is called a steady regime. For the study, a mixture of air and kerosene was used, with a reference pressure of 92,629 Pa, a reference temperature of 300 K, and a fixed speed

of 60,000 RPM. Additionally, it was assumed that the total pressure at the inlet nozzle is equal to the static pressure, as well as the pressure at the outlet nozzle being equal to ambient pressure.

The heat transfer model was based on total energy due to the high compressibility of the flow, aiming to capture temperature gradients with greater accuracy, correctly handle the coupling between compressibility and heat, and model thermal acceleration effects, such as those occurring in nozzles and combustion chambers.

The combustion model was simulated using eddy dissipation, assuming that the chemical reaction rate is limited by the turbulent mixing of reactants, rather than by chemical kinetics itself.

The boundary conditions for each element are summarized in Table 3.

Table 3 – Bounduary Conditions

Component	**Element**	**Boundary Type**
Inlet	Case	Wall
Inlet	Inlet	Inlet
Inlet	Interface with Compressor	Interface
Compressor	Blades	Wall
Compressor	Case	Wall
Compressor	Interface with Inlet	Interface
Compressor	Interface with Difuser	Interface
Difuser	Case	Wall
Difuser	Interface with Compressor	Interface
Difuser	Inetrface with Chamber	Interface
Chamber	Case	Wall
Chamber	Injector	Inlet
Chamber	Interface with Difuser	Interface
Chamber	Interface with Vanes	Interface
Vanes	Blades	Wall
Vanes	Case	Wall
Vanes	Interface with Chamber	Interface
Vanes	Inetrface with Turbine	Interface
Turbine	Blades	Wall
Turbine	Case	Wall
Turbine	Interface with Vanes	Interface
Turbine	Interface with Nozzle	Interface
Nozzle	Case	Wall
Nozzle	Interface with Turbine	Interface
Nozzle	Exhaust	Outlet

Among the various turbulence models, the k-ε model was initially chosen. This model introduces two additional transport equations: one for the turbulent kinetic energy (k) and another for its dissipation rate (ε). The turbulent kinetic energy (k) represents the amount of energy contained in turbulent motions, while the dissipation rate (ε) describes the rate at which this

energy is dissipated due to the fluid's viscosity. Solving these two equations allows the estimation of turbulence effects on the mean flow, enabling the closure of the RANS equations.

The k-ε model is widely used due to its robustness, relative simplicity, and good accuracy in various industrial and academic flow types. However, it has limitations in cases with highly anisotropic flows, severe flow separations, or significant rotational effects. It should be noted that a comparison with other models coherent with this one would be appropriate, but the limitation imposed by the student license prevented such a study.

It is also worth mentioning that, due to the model's complexity and the nodal element count limitation previously mentioned—imposed by the license granted to students by the *Ansys CFX* software—a low-fidelity simulation was performed, resulting from mesh convergence and optimization issues. Nevertheless, despite the low fidelity, the study pragmatically simulates ways to adjust models and improve efficiency in a real problem, providing significant knowledge in the use of *CFD* to reduce the consumption of an aircraft engine at a much lower cost compared to a series of wind tunnel tests — which involve high expenses due to the need for significant model modifications, the possibility of failure modes that could lead to the loss of the model itself, as well as wind tunnel rental costs, making physical testing economically unfeasible.

4.3 Simulation Convergence Criteria

The simulation stopping criterion, in general cases, is defined by the residual convergence chosen by the user; that is, the calculations converge to a solution when the residuals of the conservation equations (mass, momentum, energy, etc.) fall below a certain value, usually set to less than 10^{-4}. These residuals represent the variation of the fundamental variables of the fluid dynamics equations at each time integration step.

Since the model involves unsteady phenomena, such as large vortices in the combustion chamber, this criterion does not fully satisfy simulation convergence. The residuals for the proposed model decrease to a certain limit below 10^{-3} and then oscillate around a constant value, which is reflected as a transient regime in the variables of interest, followed by oscillations whose amplitude tends to decrease over time. This phenomenon can be observed in Figures 16 and **??**.

Figure 16 – Momentum, Mass and Total Enthalpy energy residuals

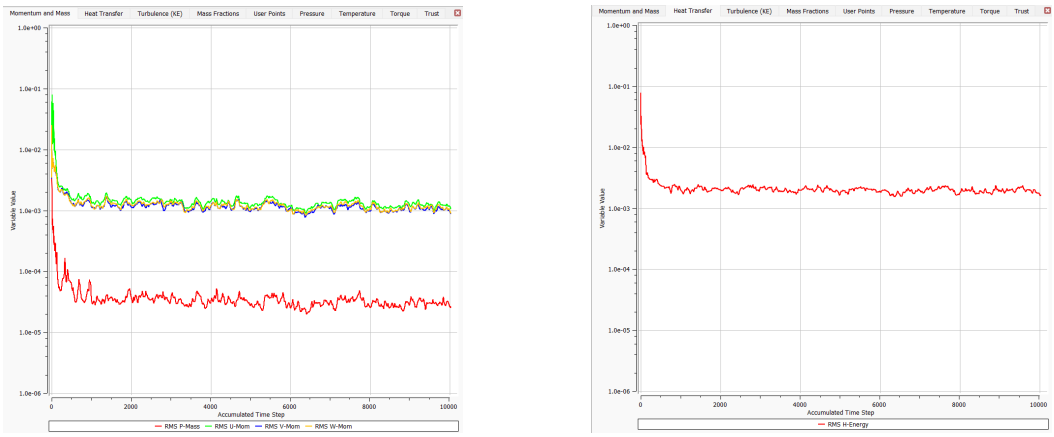

Source: Developed by the author

Figure 17 – Turbulence(Kinect Energy) and Mass fraction residuals

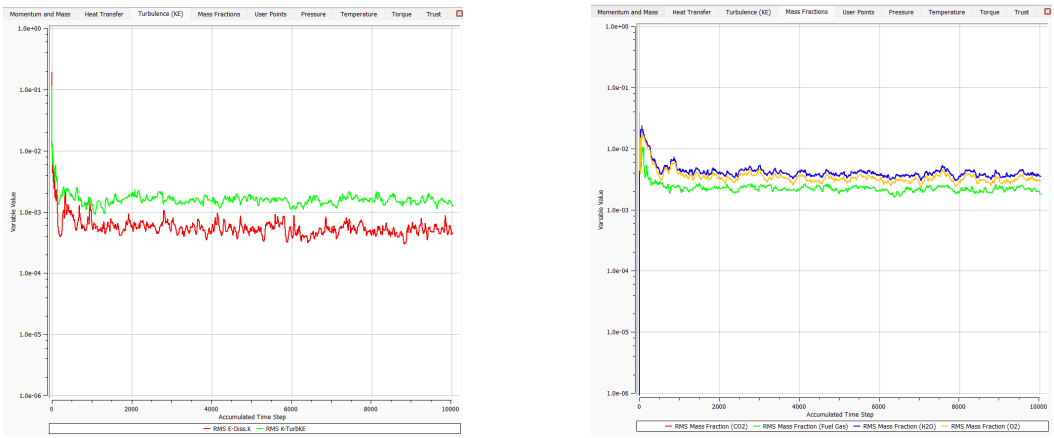

Source: Developed by the author

In this case, the physical convergence approach is used, which consists of monitoring variables of interest until they reach a regime of nearly constant oscillation: the variation is very small compared to previous steps, and it is then assumed that the value lies within a sufficiently small range so as not to interfere with the others. The monitoring parameters chosen were the torque on the compressor and turbine, thrust, exhaust temperature, and diffuser pressure, which can be seen in Figures 18 and 19.

Figure 18 – Difuser pressure and Exhaust Temperature

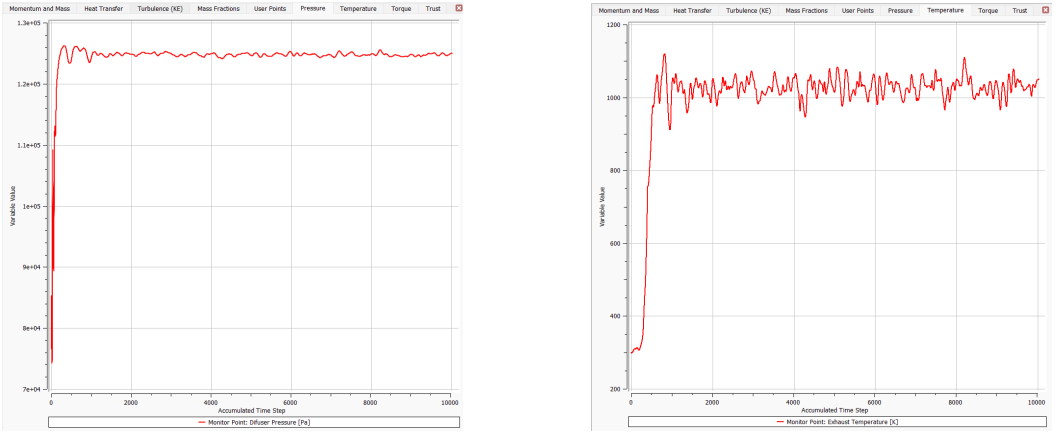

Source: Developed by the author

Figure 19 – Torque and trust of Compressor and Turbine

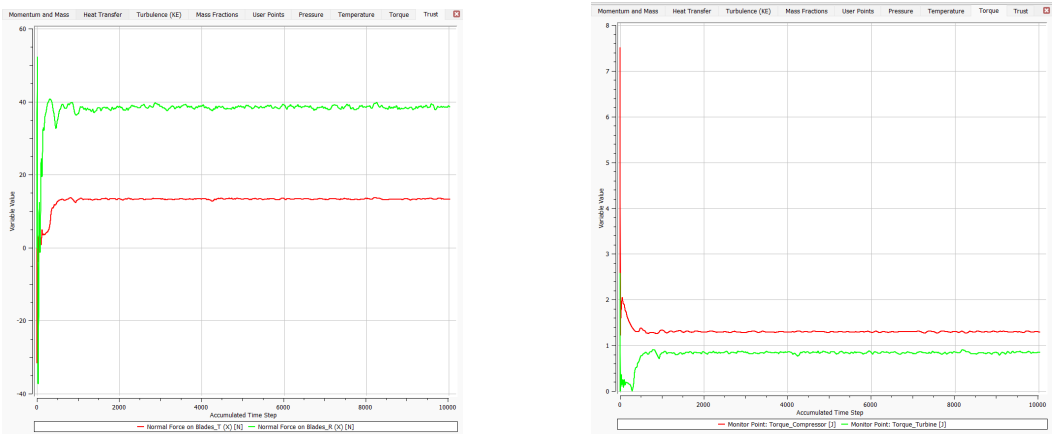

Source: Developed by the author

To obtain a small variance range among the monitored parameters, the software performed between 8,000 and 12,000 iterations per simulation, taking an average of approximately 72 hours to complete, despite the boundary conditions being chosen to reduce computational cost.

5 THEORETICAL BACKGROUND

This section presents the theoretical foundation for the performance analysis of compressors and turbines based on the book (Hill; Peterson, 1992). The objective is to model the thermodynamic and kinematic behavior of a turbine and a compressor within a propulsion system, considering energy balances, thrust, and specific fuel consumption. The Python code (available in Appendix A.1) is based on the theoretical equations presented in Chapters 7 (Compressor) and 8 (Turbine), relying on the relations developed through velocity triangles at the inlet and outlet at the mean radius of the components.

It is important to highlight that this theory assumes the fluid behavior to be well-behaved and uniform across cross-sections, thus not modeling rotational and three-dimensional effects—in other words, the flow is considered two-dimensional. Furthermore, the method does not include in its formulation the viscous effects caused by friction losses or boundary layer separation. The flow is also assumed to be fully steady.

The developed code, based on the velocity triangle concept, aims to calculate the following parameters using the velocity components, inlet temperature and pressure, radius, and constants:

- Specific work and required power
- Pressure ratio and polytropic efficiency
- Shaft torque for the compressor/turbine
- Specific fuel consumption
- Generated thrust

5.1 Modelagem do Compressor

A compressor adds energy to the flow through the work done by rotating blades. An axial compressor consists of multiple stages, each composed of a rotor (rotating blades) and a stator (stationary blades). In the case of this study, the compressor consists of only one stage, and the theoretical development is carried out specifically for a single stage and then generalized for additional stages.

For the theory, two frames of reference are considered: the absolute frame, corresponding to an observer fixed to the machine's structure, and the relative frame, which rotates with the machine. The absolute velocity is denoted by w, while the relative velocity is denoted by c, and the blade speed, denoted by U, is related to the other velocities through Equation 5.1 and can be graphically visualized in Figure 20.

$$w = c + U \tag{5.1}$$

Figure 20 – Generic Compressor Triangle of velocities

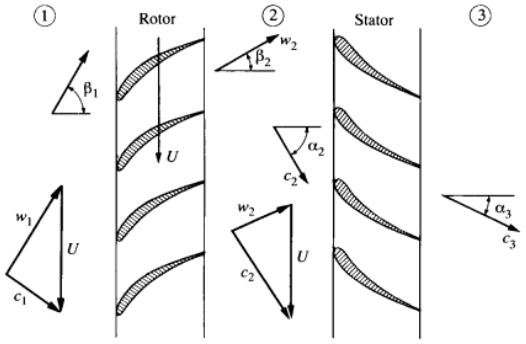

Source: Hill Peterson 1992 - Mechanics and Thermodynamics of Propulsion

The absolute flow angles are denoted by α, while β represents the flow direction relative to the rotor.

The angular momentum of the fluid is altered as it passes through the compressor blades, as a result of the pressure forces acting on the blade surfaces. The pressure on the convex side is generally relatively low, while the pressure on the concave side is typically relatively high.

Typically, the axial velocity components, denoted by c_z, vary as a function of radius. However, for simplicity, it is assumed that these components remain constant, so the velocity triangle shown in Figure 20 can be rearranged as depicted in Figure 21.

Figure 21 – Generic Compressor Triangle of velocities

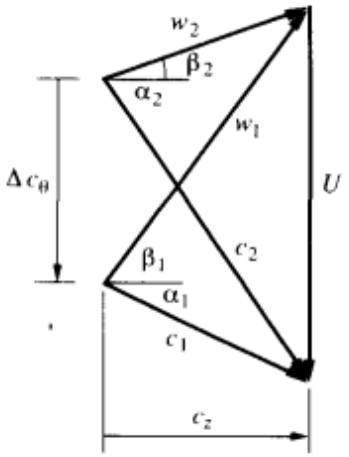

Source: Hill Peterson 1992 - Mechanics and Thermodynamics of Propulsion

Assuming that all the fluid within the rotor exhibits the kinematic behavior shown in the

figure above, and applying a control volume that encompasses only the rotor, the torque can be calculated as:

$$\tau = \dot{m}[(rC_\theta)_2 - (rC_\theta)_1] \tag{5.2}$$

Since the assumed blade speed U is constant, the power is given by:

$$\tau \cdot U = \mathcal{P}_s = -\dot{m}U(c_{\theta 2} - c_{\theta 1}), \tag{5.3}$$

The negative sign arises from the adopted convention (Hill; Peterson, 1992). Therefore, the work per unit mass done on the fluid by the rotor is:

$$w_c = \frac{\mathcal{P}}{\dot{m}} = U\Delta c_\theta \tag{5.4}$$

Since the flow is nearly adiabatic, and assuming radial stagnation enthalpy, we have:

$$0 = \dot{m}(h_0 2 - h_0 1) + \mathcal{P} \Leftrightarrow (h_0 2 - h_0 1) = U\Delta c_\theta \tag{5.5}$$

Assuming constant specific heat, a dimensionless stagnation temperature rise through the rotor can be derived from:

$$\Delta T_0 = \frac{U\Delta C - \theta}{c_p} \tag{5.6}$$

Defining the efficiency stage as:

$$\eta_{stg} = \frac{h_{03s} - h_0 1}{h_{03} - h_{01}} \tag{5.7}$$

Using the isentropic pressure–temperature relation, the pressure ratio can be written as:

$$\frac{p_{03}}{p_{01}} = \left[1 + \eta_{stg}\left(\frac{\Delta T_0}{T_{01}}\right)\right]^{\gamma(\gamma-1)} \tag{5.8}$$

Note that it is desirable to estimate the actual efficiency of the engine. However, due to model limitations and idealized conditions, the theoretical model does not yield a reasonable estimate in this regard. To overcome this issue, the turbine and compressor efficiencies provided by the manufacturer Jet Munt S.L. were used, given as 0.79 and 0.72, respectively.

5.2 Turbine Modeling

The turbine modeling is analogous to that of the compressor, but with the opposite convention regarding power and parameter indices.

5.2.1 Thrust

The thrust reaction $\mathcal{T}$ transmitted through the structural support is illustrated in Figure 22.

Figure 22 – Generalized thrust-producing device

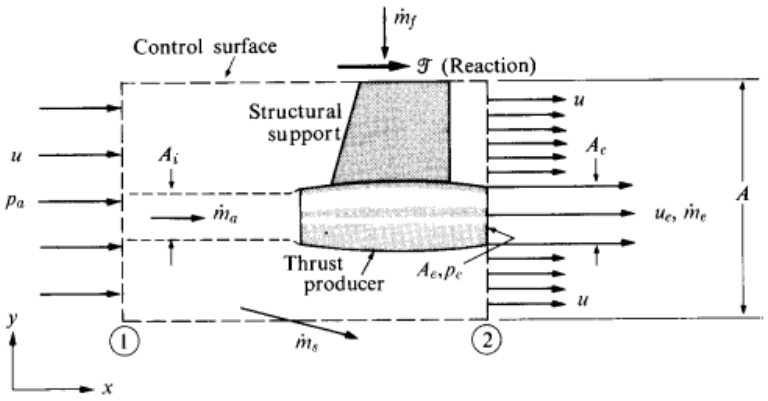

Source: Hill Peterson 1992 - Mechanics and Thermodynamics of Propulsion

In this context, the engine thrust can be defined as the vector sum of all forces acting on the internal and external surfaces of the engine and nacelle. The thrust of the generalized thrust generator can be derived from Equation 5.9 by applying it to a steady-state flow:

$$\sum F = \int u\rho(u \cdot n)dA \tag{5.9}$$

Para a direção x, tem-se:

$$\sum F_x = \int u_x\rho(u \cdot n)dA \tag{5.10}$$

Assuming reversible external flow, both pressure and velocity can be considered constant across the entire control surface, except at the exhaust area A_e of the engine. If the exhaust velocity u_e is supersonic, the exhaust pressure p_e may differ from the ambient pressure p_a. The net pressure force on the control surface is therefore $(p_a - p_e)A_e + \mathcal{T}$. The only other force acting on this control volume is the thrust reaction. Summing the forces on the control surface acting in the x-direction, we obtain:

$$\sum F_x = (p_a - p_e)A_e + \mathcal{T} \tag{5.11}$$

The mass flow through the control volume is given by:

$$\dot{m}_a = \rho u A_i \quad \text{(captured air)} \tag{5.12}$$

$$\dot{m}_e = \rho_e u_e A_e \quad \text{(exaustion gas)} \tag{5.13}$$

$$\dot{m}_f = \dot{m}_e - \dot{m}_a \quad \text{(fuel)} \tag{5.14}$$

From the continuity equation for the control volume:

$$\int_{cs} \rho \mathbf{u} \cdot \mathbf{n} \, dA = 0 \tag{5.15}$$

Which expands to:

$$\rho_e u_e A_e + \rho u (A - A_e) + \dot{m}_s - \dot{m}_f - \rho u A = 0 \tag{5.16}$$

Where $\dot{m}_s$ is the airflow through the lateral surfaces. Rearranging:

$$\dot{m}_s = \dot{m}_f + \rho u A_e - \rho_e u_e A_e \tag{5.17}$$

Substituting Equation (5.14) into (5.17):

$$\dot{m}_s = \rho u (A_e - A_i) \tag{5.18}$$

the net momentum flux in the x-direction is:

$$\begin{aligned} \int_{cs} u_x \rho (\mathbf{u} \cdot \mathbf{n}) \, dA = \dot{m}_e u_e + \dot{m}_s u + \rho u (A - A_e) u \\ - \dot{m}_s u - \rho u (A - A_i) u \end{aligned} \tag{5.19}$$

Simplifying and using Equation (5.18):

$$\int_{cs} u_x \rho (\mathbf{u} \cdot \mathbf{n}) \, dA = \dot{m}_e u_e - \dot{m}_a u \tag{5.20}$$

Equating Equations (5.11) and (5.20):

$$(p_a - p_e) A_e + \mathcal{T} = \dot{m}_e u_e - \dot{m}_a u \tag{5.21}$$

Isolating $\mathcal{T}$ and expressing $\dot{m}_e = \dot{m}_a + \dot{m}_f$:

$$\mathcal{T} = \dot{m}_a (1 + f) u_e - \dot{m}_a u + (p_e - p_a) A_e \tag{5.22}$$

Where $f = \dot{m}_f / \dot{m}_a$ is the fuel-to-air ratio.

5.3 Specific Fuel Consumption (SFC)

Since the fuel mass flow is empiric, the specific guel conumption is defined as:

$$SFC = \frac{\dot{m}_{fuel}}{F} \quad \text{[kg/N.s]} \tag{5.23}$$

6 EFFICIENCY IMPROVEMENTS METHODS

As previously presented, in a second phase, the study explored the capability of the turbojet engine model to increase the overall engine efficiency, that is, to maintain or increase thrust production while reducing fuel consumption. Among the components of the design, the turbine and the combustion chamber showed the greatest potential for efficiency gains in the model, and therefore were chosen for optimization. The reasoning adopted for reducing fuel consumption is developed below.

6.1 Combustion Chamber

The optimization performed on the combustion chamber consisted of gradually increasing the size of the air inlet holes, making the air-kerosene mixture richer, thus adding more energy to the fluid. The obvious problem with this approach is the limitation of the hole size, which can cause air recirculation to the previous stages, creating a wake blockage that results in a significant efficiency loss.

To mitigate this limitation, several simulations were performed with gradual increases of 5 to 10 percent in the size of all holes, until an efficiency increase was achieved without causing any recirculation in the model. A saturation of this method was noted for the largest holes, located in the central part of the chamber, at around a 25% increase — meaning that an increase beyond this dimension resulted in recirculation and consequently an increase in fuel consumption to achieve torque equilibrium between the turbine and compressor. However, the other holes showed a delayed saturation: up to a 35% increase in diameter yielded efficiency gains in the model. The resulting diameters from this method can be seen in Table 4.

Table 4 – Final diameters of combustion chamber air injector

Air injector number	Final diameter [mm]
1	1.35
2	1.35
3	2.50
4	3.75
5	1.35

6.2 Turbine

For the turbine, the approach was based on the flow generated around the blades. To avoid flow separation, it is desired that the streamlines remain parallel to the airfoil contour. Moreover, it is known that there is a linear range of angles for which lift and drag increase due

to higher incidence. With this in mind, the turbine blade incidence was gradually increased to analyze the flow behavior caused by this change.

With a 7-degree increase, the flow remained attached to the airfoil, showing the maximum efficiency observed in the range from 1 degree to 8 degrees, while the 8-degree increment presented an efficiency loss caused by the onset of flow separation, which will be further explored in the results section. The comparison between the airfoils can be seen in Figure 23. The final geometry obtained can be observed in Figure 24.

Figure 23 – Increase of 7 degress and original angle of attack of the turbine airfoil

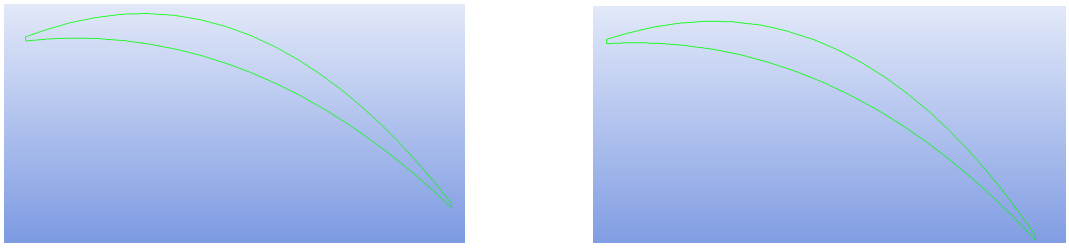

Source: Developed by the author

Figure 24 – Final geometry of turbine

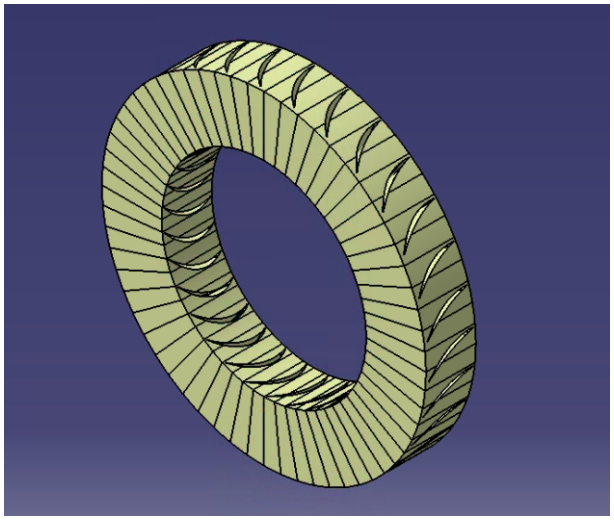

Source: Developed by the author

7 REAL ENGINE MODEL

According to (Jets Munt SL, 2011), the engine operation begins with the start-up sequence, which is controlled by an electronic unit that initiates the ignition procedure and monitors the engine parameters within design limits.

The engine uses a direct liquid fuel preheating system, ignited by a long-lasting ceramic ignition plug installed internally. After the initial preheating, the liquid fuel is gradually introduced.

The fuel must contain a small percentage (4%) of oil, part of which is used to lubricate the two high-speed ceramic bearings.

Fuel is supplied to the engine from a tank through a small electric pump. The engine speed, from idle to maximum, is controlled by varying the fuel pump speed via an electronic controller called the ECU (Electronic Control Unit).

The manufacturer's motor specifications are given in Table 5.

Table 5 – Merlin 90 Turbojet Specifications

Dimensions	Outer diameter: 90 mm, Length: 230 mm
Total Mass	1150 g
Rated Thrust (15 °C, sea level)	Greater than 90 Newtons
Maximum RPM	152,000
Idle RPM	42,000
Thrust at idle	4 Newtons
Exhaust Gas Temperature	550–650 °C
Fuel Consumption	0.33 L/min at 90 Newtons
Fuel	Kerosene + 4% oil (3%–5% acceptable)
Oil	100% synthetic 2-stroke motorcycle oil or turbine oil

Source: Jets Munt SL. *Merlin 90/100/140/160 Instruction Manual*, Version 3.1/2011, p. 5. Available at: jets-munt.com

For a rotation speed of 60,000 RPM, the engine requires a consumption of 2.44 $\frac{g}{s}$ of kerosene.

8 EXPERIMENTAL DATA

As mentioned, the Department of Aeronautical Engineering holds the Merlin 90 model, and the professor and advisor of this study, Dr. Paulo Greco, conducted bench tests, extracting data from the turbojet. The engine was tested at three different speeds: 35,000, 50,000, and 60,000 RPM. The data obtained are reproduced in Table 6.

Table 6 – Experimental data for 60000 RPM

Parameter	**60000 RPM**	**50000 RPM**	**40000 RPM**	**35000 RPM**
T_a [K]	300	299	299	299
T_2 [K]	315	310	308	306
T_3 [K]	343	332	327	325
T_5 [K]	890	900	926	957
P_a [Pa]	92629	92631	92636	92666
P_2 [Pa]	89519	90661	91364	91861
P_3 [Pa]	123757	113405	106498	102214
P_5 [Pa]	94680	94046	93636	93392
m_f [g/s]	2,44	2,06	1,56	1,44
Trust [N]	23	15	11	6
Specific trust [$\frac{N \cdot g}{s}$]	9,4	7,35	7,05	4,17

The typical efficiencies of each component are within the range shown in Table 7 (Hill; Peterson, 1992).

Table 7 – Typical values of stage efficiencies

Parameter	**Range**
η_d	0.7 to 0.9
η_c	0.85 to 0.9
η_t	0.9 to 0.95
η_n	0.95 to 0.98
η_b	0.97 to 0.99

According to the engine manufacturer, the efficiencies n_t and n_c are 0.79 and 0.72, respectively, which differ significantly from the typical values, as expected, since this engine requires a lower efficiency than general aviation.

In a basic thermodynamic analysis, using the efficiencies provided by the manufacturer and the other efficiencies as typical values (Hill; Peterson, 1992), shown in Table 8, and using the experimentally obtained input data, the following parameters were obtained, as shown in Table 9.

Table 8 – Assumed efficiencies of other stages

Parameter	Value
η_b	0,97
η_n	0,98
η_d	0,7

Table 9 – Thermodynamics Analysis with typical and manufacturer efficiencies

Parameter	60000 RPM	50000 RPM	40000 RPM
T_6 [K]	779	759	893
M_2 [-]	0,14	0,04	0,07
M_3 [-]	0,64	0,54	0,45
M_5 [-]	0,37	0,29	0,17
M_6 [-]	0,41	0,33	0,21
T_02 [K]	316	311	308
T_03 [K]	371	352	341
T_04 [K]	884	848	802
T_05 [K]	805	793	765
P_02 [Pa]	90776	90778	91709
P_03 [Pa]	162596	138273	122381
P_05 [Pa]	103996	99792	95599
V_2 [m/s]	50	15	26
V_3 [m/s]	237	197	163
V_6 [m/s]	229	183	117
Trust [N]	35	24	12
Specific trust [$\frac{N \cdot g}{s}$]	14,3	11,6	7,7

The efficiencies adopted in the 35,000 RPM analysis resulted in negative velocities, indicating recirculation, which made the other parameters unsuitable for analysis, and therefore the data were omitted. It is also noted that the theoretical thrust values obtained differ significantly from the experimental test results, indicating that the real engine has a lower efficiency, and thus, the efficiencies of each stage must be lower than the typical values shown in Table 7.

In order to balance the experimental and theoretical torques, the efficiencies shown in Table 10 were used. The data obtained by applying the same analysis are reproduced in Table 11.

Table 10 – Assumed stage efficiencies

Parameter	Range
η_d	1.0
η_c	0.7
η_t	0.64
η_n	0.9
η_b	0.96

Table 11 – Thermodynamics Analysis with assumed efficiency

Parameter	**60000 RPM**	**50000 RPM**	**40000 RPM**	**35000 RPM**
T_6 [K]	909	921	893	918
M_2 [-]	0,22	0,18	0,14	0,11
M_3 [-]	0,64	0,54	0,45	0,38
M_5 [-]	0,26	0,23	0,12	0,03
M_6 [-]	0,32	0,27	0,17	0,11
T_02 [K]	318	312	309	307
T_03 [K]	371	352	341	334
T_04 [K]	1005	988	934	945
T_05 [K]	927	935	898	920
P_02 [Pa]	92629	92631	92636	92666
P_03 [Pa]	162596	138273	122381	112810
P_05 [Pa]	99304	97545	94529	93456
V_2 [m/s]	79	62	49	39
V_3 [m/s]	237	197	163	137
V_6 [m/s]	191	166	102	67
Trust [N]	30	22	11	6
Specific trust [$\frac{N \cdot g}{s}$]	12,3	10,7	7,05	4,17

It is noticeable that there still exists a divergence between the theoretical and experimental torques, especially at higher rotational speeds. At higher speeds, the effects of non-idealities, propulsive efficiency losses, aerodynamic losses, and thermal losses become more significant and are not adequately captured by the theoretical model. Consequently, larger discrepancies are observed at higher rotational speeds.

9 RESULTS

This chapter presents the results obtained in the study, as well as the discussion and interpretation of them.

9.1 Physical incongruence Validation

The study began with the identification of a physical inconsistency presented as a significant difference in the torques generated by the compressor and the turbine, constituting an absurdity in the simulation and a lack of balance between the components, which by design are connected by a single shaft and therefore should have very similar torques.

Among the approaches mentioned in the problem description, the one that proved to be the most responsive and efficient was the gradual increase of fuel injection in the combustion chamber. The effect of this approach can be seen in Figure 25.

Figure 25 – Fuel injection relation with the diffrence of torque between turbine and compressor

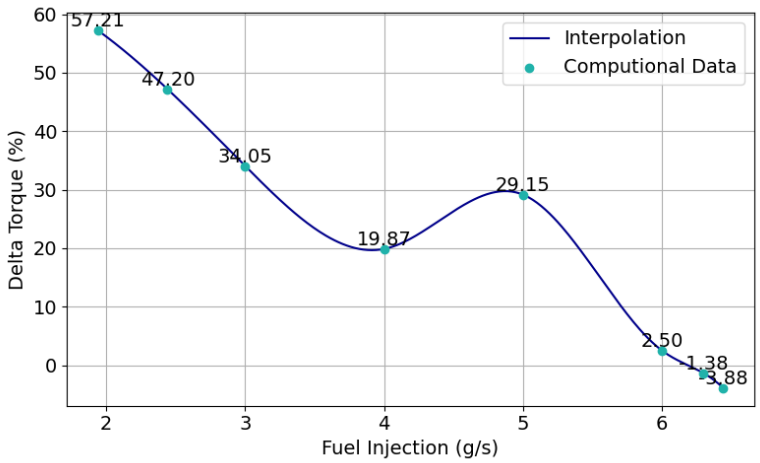

Source: Developed by the author

It can be seen from Figure 25 that the fuel consumption required by the computational model at 60,000 rpm is around 6.2 grams per second, approximately 250% less efficient than the real turbojet, which was expected since much of the computational model's geometry was idealized, in addition to the inherent limitations of the *CFX* software.

However, Figure 26 shows that the specific thrust—thrust per gram of injected fuel—decreases, being 51% lower compared to the original engine; that is, the computational model is about twice as inefficient as the Merlin 90 turbojet.

Figure 26 – Especific trust

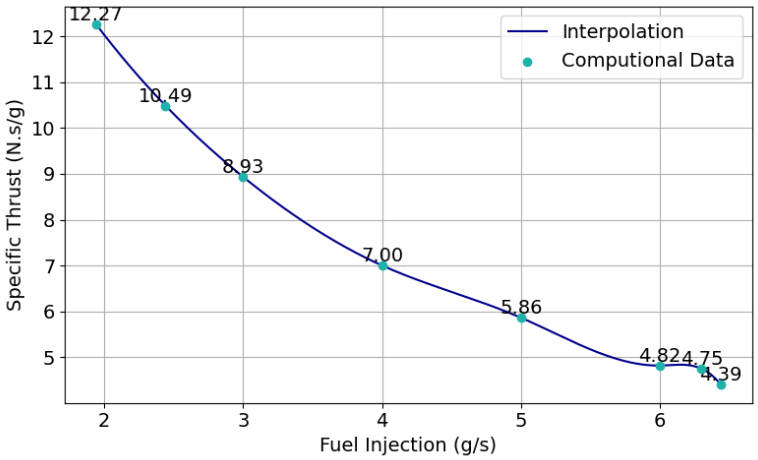

Source: Developed by the author

Furthermore, with great assistance from the advising professor, the behavior of the engine at other rotational speeds was studied, obtaining the results shown in Figure 27.

Figure 27 – RPM relation with thrust

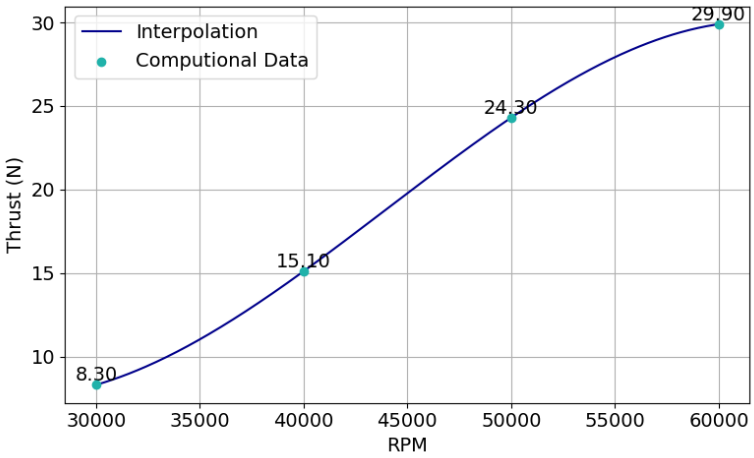

Source: Developed by the author

It is noted that the thrust generated by the turbojet also increases with the increase in engine speed, which was expected, since the increased air intake allows for a more energetic combustion, causing the gases to be ejected from the engine at a higher velocity.

Furthermore, for the rotational speeds of 30,000 RPM, 40,000 RPM, and 50,000 RPM, the torque balance between the turbine and compressor was achieved at 2.5 g/s, 3.5 g/s, and 4.6 g/s respectively, obtaining the specific thrust shown in Figure 28.

Figure 28 – RPM relation with specific thrust

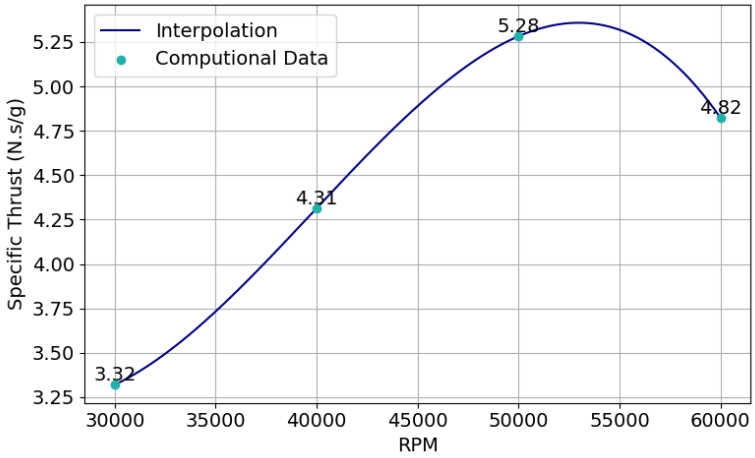

Source: Developed by the author

9.2 Efficiency Improvements

The approaches described in Chapter 6, applied to the compressor and turbine, brought efficiency gains to the engine. The following section discusses the optimization of the turbine and combustion chamber.

9.2.1 Turbine Efficiency Improvements

For the turbine, an increase in the angle of attack relative to the original airfoil was implemented. The progression of angles had the effects shown in Figures 29 and 30.

Figure 29 – Increase of attack angle and trust relation

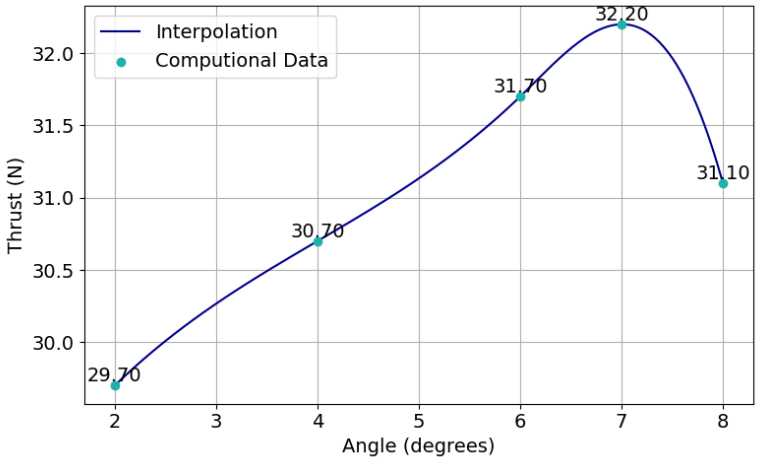

Source: Developed by the author

Figure 30 – Increase of attack angle and specific trust relation

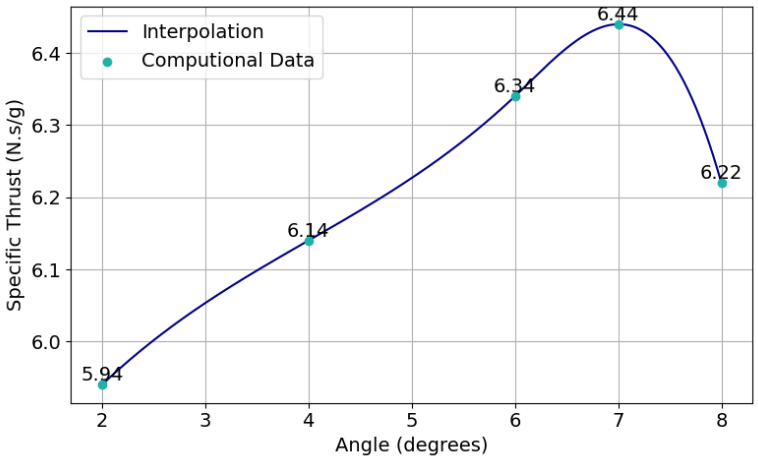

Source: Developed by the author

It can be observed from the figures above that there is a progression of thrust with the increase in angle of incidence up to approximately 7 degrees. Beyond 7 degrees, the thrust generation curve declines, indicating a loss of efficiency, which is very similar to the stall of an airfoil if the measured quantity were lift. The stall phenomenon causes an abrupt loss of lift due to boundary layer separation; therefore, this effect was studied in the turbine.

The flow separation phenomenon on a surface can be caused by various factors, such as roughness which can cause separation bubbles, highly complex surfaces, but one of the most common causes is high incidence angle, which can lead to abrupt stall of the element depending on the adverse pressure gradient generated. In the case of a turbojet engine, boundary layer separation can result in local loss of work, loss of heating, unstable flows, internal shock waves, among other factors that reduce engine efficiency. However, visualizing separation is a phenomenon that is still complex to capture in experimental tests, being possible only under very controlled conditions and relatively low speeds compared to aircraft operation. One of the advantages of CFD simulation over wind tunnel testing is precisely the ability to reproduce fluid behavior on surfaces through visual methods, providing a complementary tool to the pressure distribution on the element—as is typically identified in wind tunnel tests.

One way to obtain this type of visualization is by creating a velocity field directly on the element, checking for regions of zero velocity. The velocity distribution can be observed on the turbine blades in Figure 31.

Figure 31 – Velocity distribution arround the Turbine

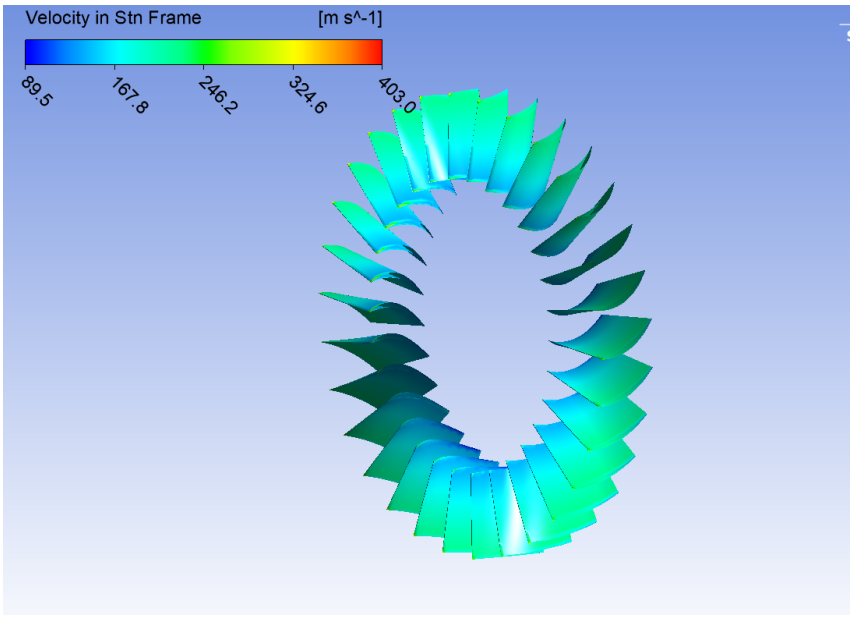

Source: Developed by the author

A smooth velocity gradient can be observed in the figures, without abrupt drops along the entire surface; however, there are no clear visual indications evidencing possible separation. In order to better analyze the flow behavior on these surfaces, a plane was created at the mid-section of both elements, and velocity streamlines were plotted on this plane, simulating the direction of airflow around the turbine blades. The result can be seen in Figure 32.

Figure 32 – Streamlines arround the Median Section of the Turbine

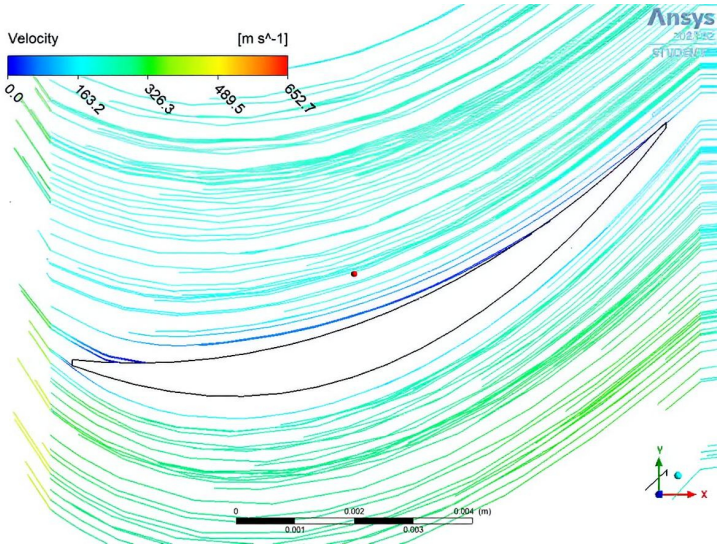

Source: Developed by the author

For the calculation of the angle of attack, the *Ink Scape* software was used, and through simple trigonometric relations, an incidence angle of approximately $53°$ for the turbine was obtained, as shown in Figure 33.

Figure 33 – Angle of Attack of Compressor of Turbine

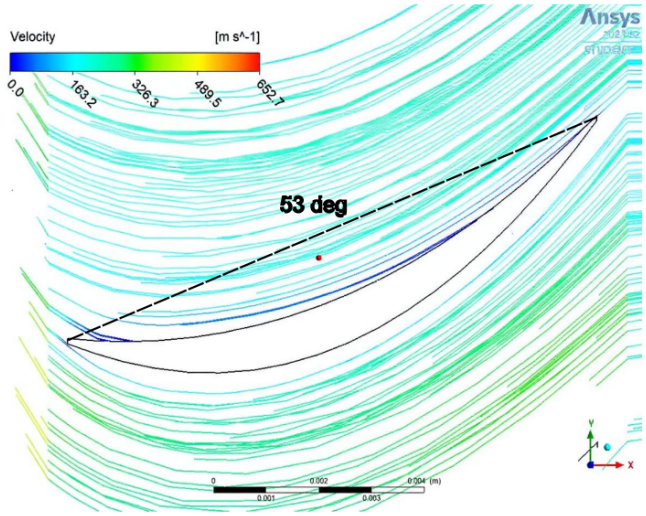

Source: Developed by the author

It is noted that the angle of incidence on the turbine is quite sharp, and although there is evidence that the flow adheres well to the airfoil contour as shown in Figure 32, there remains some uncertainty as to whether boundary layer separation actually occurs in the turbine.

Aiming for a more precise analysis of this phenomenon, the pressure distribution on a turbine blade element was plotted on the streamline plane, which can be seen in Figure 34.

Figure 34 – Pressure distribuiton arround turbine airfoil

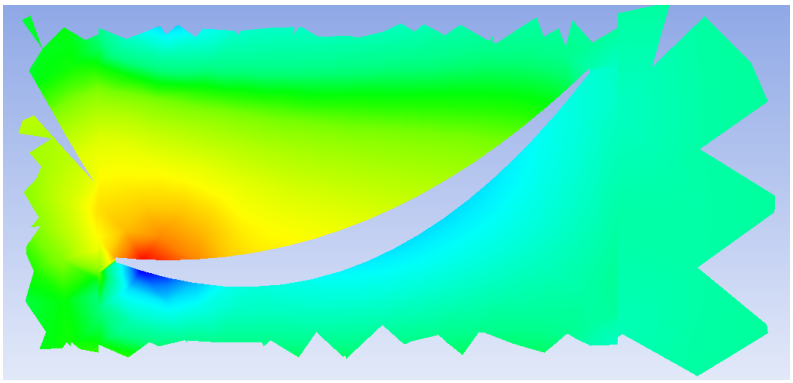

Source: Developed by the author

From Figure 34, a possible indication of flow separation onset near the trailing edge on the suction side can be observed, which explains the efficiency drop for turbine airfoil incidence angles greater than 7 degrees, as shown in Figure 30, since beyond this angle a separation zone would develop in this region.

To support this argument, the pressure coefficient distribution on this blade element was also plotted, which is shown in Figure 35.

Figure 35 – Pressure coefficient distribution for turbine airfoil

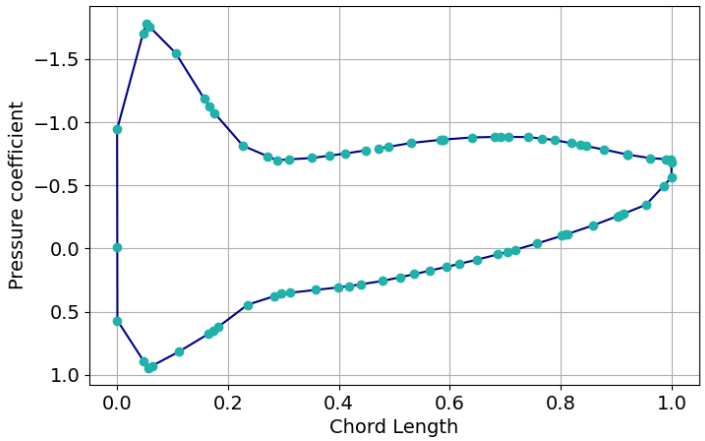

Source: Developed by the author

9.2.2 Compressor Bonduary Separation

One of the most critical elements regarding boundary layer separation is also the compressor, and therefore it was decided to check for boundary layer separation for a possible critical optimization, using a methodology analogous to that of the turbine. Thus, the velocity distribution is shown in Figure 36.

Figure 36 – Velocity distribution arround the Compressor

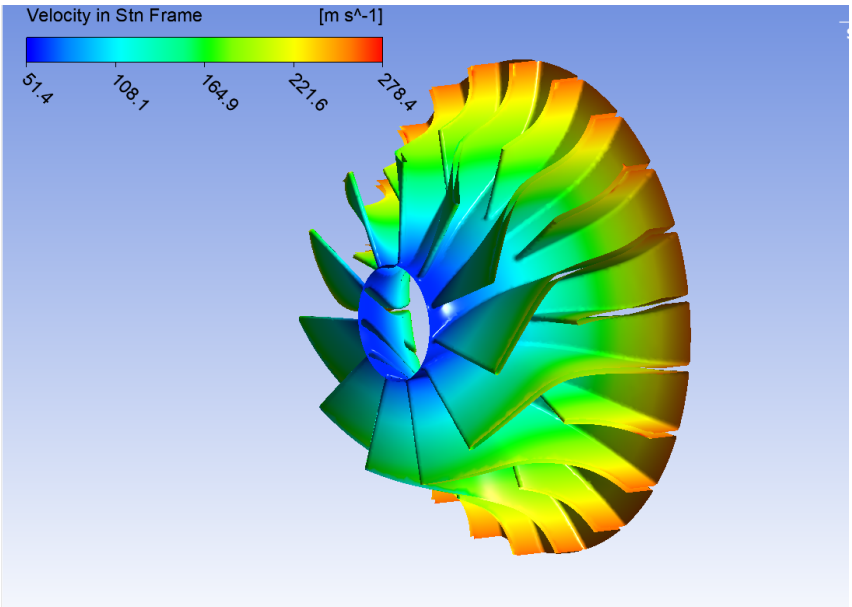

Source: Developed by the author

Similarly, in order to better investigate the separation phenomenon, the velocity streamlines in the mid-section of the compressor are shown in Figure 37.

Figure 37 – Streamlines arround the Median Section of the Compressor

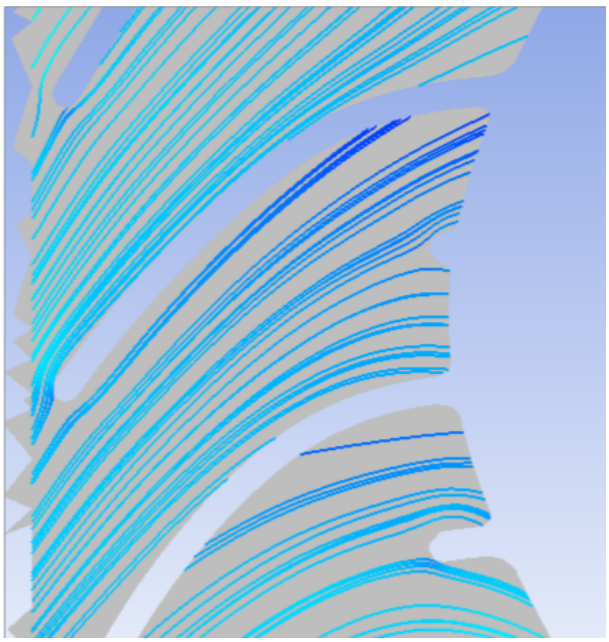

Source: Developed by the author

For the compressor, there is no defined airfoil, since geometric twists make it impossible to fully represent the airfoil bidimensionally, as it is a section of a 3D blade. Therefore, the mean camber line of the section was used, analogous to a chord line, resulting in an angle of approximately $3°$, as shown in Figure 38.

Figure 38 – Angle of Attack of Compressor

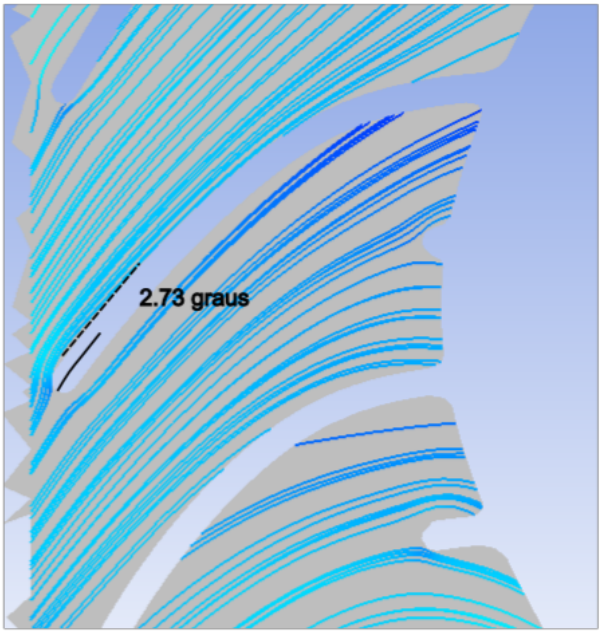

Source: Developed by the author

It can be noted from the figure that the flow is well-behaved, adhering closely to the surrounding surface, which indicates that the flow remains attached and thus rules out the possibility of significant and apparent separation. This fact justifies why the compressor was not considered as an element for optimizations with significant effects, although it certainly can be explored in future research.

9.2.3 Combustion Chamber Improvements

The approach adopted in the combustion chamber was similar; the gradual increase in the diameter of the air inlet holes produced the effect shown in figures 39 and 40.

Figure 39 – Increase of diameter and trust relation

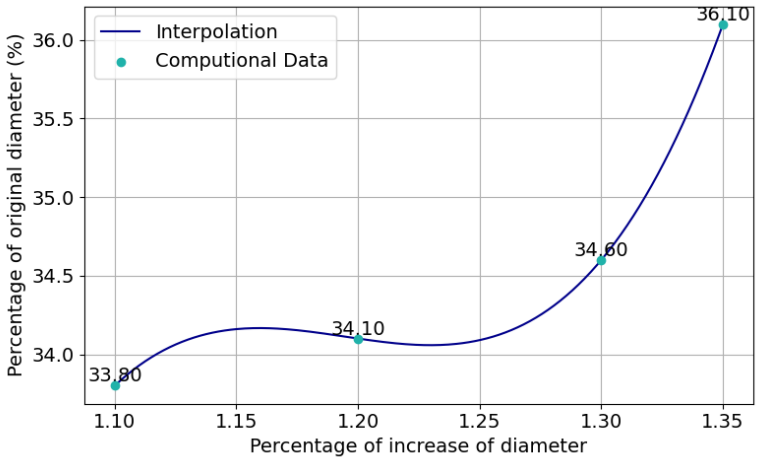

Source: Developed by the author

Figure 40 – Increase of diameter and specific trust relation

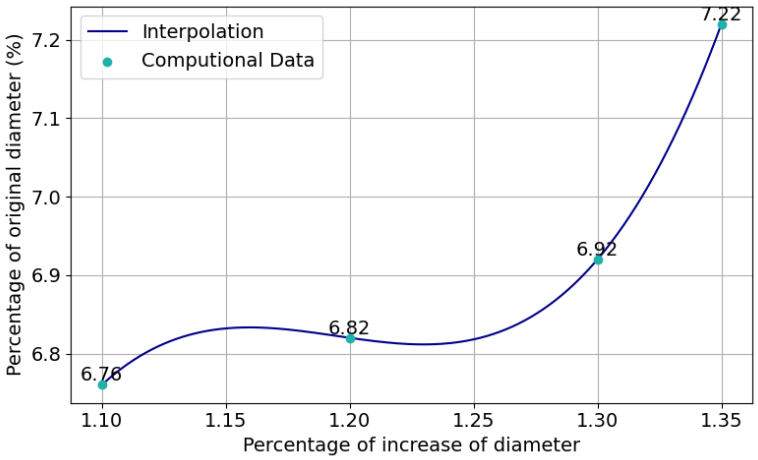

Source: Developed by the author

It is noted from the above figures that the engine generates greater torque with the increase in diameter, almost exponentially. It is worth recalling that, as mentioned, beyond a 25% increase in diameter, only the smaller holes were subject to enlargement, since the larger central holes exhibited recirculation. It is also pertinent to highlight that explorations of larger increments were limited by the educational license of *Ansys CFX*.

The final version was also simulated with an injection value of 4.5 g/s, obtaining a torque difference ratio between turbine and compressor of less than 5%, considered acceptable, producing 36.5 N of thrust, resulting in a specific consumption of approximately 8.11 $\frac{N \cdot g}{s}$. Thus, with the implemented modifications, a geometry 168% more efficient than the original geometry was achieved, reaching an efficiency very close to the studied model (about 83.3% of the real turbojet).

As with the turbine and compressor, one of the main causes of increased fuel consumption was also explored. Another phenomenon intrinsically related to efficiency loss is the existence of significant reverse flow in the combustion chamber. If the flow returns to the external region of the combustion chamber, thi

Figure 41 – Recirculation inspection of three different section on the combustion chamber: front, center and back

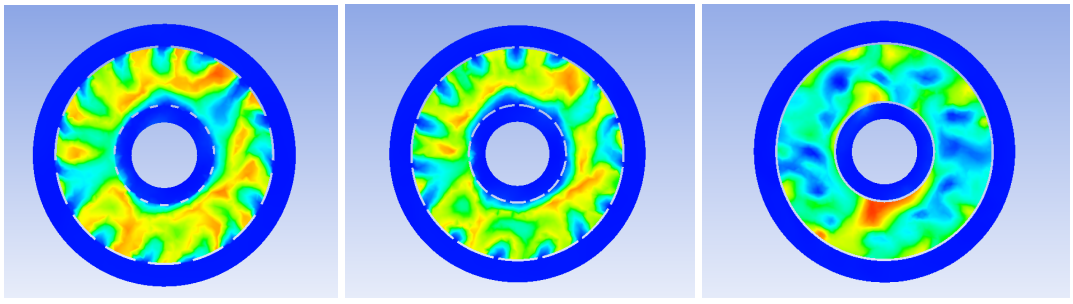

Source: Developed by the author

From the figure above, it can be inferred that since the fluid does not return to the external region of the combustion chamber, there is no significant recirculation in the turbojet, thus eliminating hypotheses of efficiency loss due to this phenomenon.

9.3 Experimental, Theorethical and CFD comparison

For the theory developed in Chapter 5, the equations were implemented in a Python *script*, which can be found in Appendix A.1. The obtained results are reproduced in Table 12. Additionally, the results obtained from the CFD simulations were reproduced, as well as those from the thermodynamic analysis conducted by the supervising professor of this study.

Table 12 – Script results with basic thermodynamics and CFD comparison

Parameter (unit)	**Value (script)**	**Value (basic thermodynamics)**	**Value (CFD)**
PR_c [-]	1.38	1.76	1.72
T_{03} [K]	357	371	360
p_{03} [Pa]	139295	162596	162309
p_{04} [Pa]	105193	–	126457
T_{04} [K]	1044	1005	1514
PR_t [-]	1.11	–	1.19
T_{05} [K]	1020	927	1511
V_6 [m/s]	113	191	294
M_6 [-]	0.18	0.32	–
T_6 [K]	1013	909	–
$Thrust$ [N]	21.3	30	36.5

It is noted that the values diverge increasingly as the stages progress, which is justifiable between the first two approaches due to the physical and mathematical modeling, as well as the difference in adopted efficiencies. In the first case, the turbine and compressor efficiencies were taken as those provided by the manufacturer, while the second theory involved greater idealization. The differences observed in the CFD-simulated engine were expected and arise from the differences and idealizations in the construction of the computational model, as well as the presence of fewer idealized assumptions.

However, it is worth highlighting that the theory developed in the script (Hill; Peterson, 1992) showed a better approximation to the real case in terms of thrust, being about 1.7 Newtons lower at 60,000 RPM, but it generates a lower exit velocity as well as nearly all other parameters, which may lead to structural underestimation of the model.

Among the several calculated parameters, the power of the turbine and compressor was modeled by the script as well as by the CFD data. With the force calculation, it was also possible to compute the SFC in both approaches. The results obtained can be seen in Table 13.

Table 13 – Power and SFC comparison

Method	SFC [$\frac{kg}{N \cdot s}$]
Script	0.114
CFD	0.123

It is noted in both cases an apparent great similarity in the specific fuel consumption, since small differences in this parameter translate into large differences in efficiency.

Finally, out of curiosity, an experiment was conducted using the fuel and air intake data identical to those used in the simulation, 4.5 g/s of fuel and 119 g/s of air, which resulted in a thrust of 23.07 N and an SFC of 0.119 $\frac{kg}{N \cdot s}$, closely approaching the experimental thrust, evidencing the sensitivity of the theoretical model to the mass flow rates.

10 CONCLUSION

This study is introduced by highlighting the importance of making aviation more sustainable, which can be achieved through various approaches, given that an aircraft is a multidisciplinary product. This concern is directly linked to improving the efficiency of aircraft, as well as the adoption of propulsion systems powered by non-polluting fuels, the latter being an expected approach for commercial and executive aviation by 2050.

Regarding the reduction of fuel consumption in aircraft, computational simulation tools such as CFD have proven to be a practical and less costly alternative compared to design modifications that would require wind tunnel testing to validate even the smallest changes. The flexible modification of the computational model allows for much greater design volatility, as well as avoiding the waste of reworking parts for wind tunnel tests or flight test campaigns. Moreover, the simulation environment permits multiple experimental runs without the risk of damaging any component.

In this study, the focus was on reducing fuel consumption of a turbojet engine, one of the main components of an aircraft, using CFD simulation. Initially, a real engine model was used as the basis for creating a computational model. However, it was noted that the geometric idealizations generated a significant difference between the engines, which even resulted in a physical inconsistency due to the different required fuel intake rates by the computational model; that is, the constructed turbojet was less efficient than the real one.

To overcome this discrepancy, the fuel injection rate that balanced the torques between the compressor and turbine was found. With the model stabilized, optimization of the modeled engine was carried out. Focusing on two components—the turbine and combustion chamber—the demonstrated approaches produced significant effects on the specific thrust generation, reaching an operation close to the baseline model and increasing the computational model efficiency by approximately 160

Continuing the analysis, some theories were compared with the virtual model despite the differences. From the various approaches used, it was concluded that they are complementary and, when used together, promote a more efficient turbojet design tailored to the desired operating conditions. Furthermore, scholars of this study are encouraged to venture into proposing optimization strategies for other components, since the main focus of this work was on two elements.

Finally, it is emphasized the effectiveness demonstrated by CFD as an alternative for optimization that cannot be fully quantified but is perceived to be much more cost-effective than optimization via experimental simulation, although one approach does not exclude the other.

REFERENCES

AGÊNCIA INTERNACIONAL DE ENERGIA. **U.S. and International Commitments to Tackle Commercial Aviation Emissions**. 2025. Discussão sobre compromissos dos EUA e internacionais para reduzir emissões da aviação comercial. Available at: https://www.eesi.org/articles/view/u.s-and-international-commitments-to-tackle-commercial-aviation-emissions. Access at: 29 abr. 2025.

AVIATION WEEK. **E190-E2 Offers 17.3% Fuel Burn Reduction, 11% From Engine Alone**. 2025. Comparativo técnico da eficiência por motor. Available at: https://aviationweek.com/air-transport/aircraft-propulsion/embraers-e190-e2-cuts-fuel-burn-173-11-engines. Access at: 29 abr. 2025.

HILL, P. G.; PETERSON, C. R. **Mechanics and Thermodynamics of Propulsion**. 2nd. ed. Reading, Massachusetts: Addison-Wesley, 1992. Classical reference on propulsion systems, widely used in aerospace engineering.

Jets Munt SL. **Merlin 90/100/140/160 Instruction Manual**: Version 3.1/2011. Arenys de Munt, Barcelona, Spain, 2011. Gas turbine engine manual for RC applications. Available at: https://www.jets-munt.com. Access at: 29 abr. 2025.

MERCADO & EVENTOS. **Combustível se torna um desafio: indústria aérea gastará US$ 291 bi em 2024, 32% dos custos**. 2024. Dados sobre custos de combustível na aviação em 2024. Available at: https://www.mercadoeeventos.com.br/noticias/aviacao/. Access at: 29 abr. 2025.

ORGANIZAÇÃO DA AVIAÇÃO CIVIL INTERNACIONAL. **CORSIA – Carbon Offsetting and Reduction Scheme for International Aviation**. 2025. Informações oficiais sobre o programa CORSIA. Available at: https://www.icao.int/environmental-protection/CORSIA. Access at: 29 abr. 2025.

APPENDIX

APPENDIX A – PYTHON SCRIPT

```
import numpy as np
import matplotlib.pyplot as plt
import math as m
from scipy.interpolate import make_interp_spline

# Constants
gamma = 1.4
R = 287
cp = 1005
fuel_heating_value = 43e6

# Efficiencies
eta_c = 0.72
eta_t = 0.79

# Experimental data
Ta = 300; T2 = 315; T3 = 343; T5_exp = 890
pa = 92629; p2 = 89519; p3 = 123757; p5 = 94680
mf = 0.0045     # Real fuel mass flow (kg/s)
ma = 0.119      # Real air mass flow (kg/s)
A6 = 1.884e-3   # Nozzle area (m²)

# 1. Compressor calculations
PR_comp = p3/p2
T3s = T2 * (PR_comp)**((gamma-1)/gamma)
T03 = T2 + (T3s - T2)/eta_c
p03 = p2 * (T03/T2)**(gamma/(gamma-1))
Wc = cp * (T03 - T2)

# 2. Combustor
f = mf / ma
T04 = (mf * fuel_heating_value)/(ma * cp) + T03
p04 = p3 * 0.85  # 15% pressure loss

# 3. Turbine calculations
PR_turb = p04/p5
ER_turb = (p5/p04)**(1/gamma)  # Expansion ratio
T5s = T04 * (1/PR_turb)**((gamma-1)/gamma)
T05 = T04 - eta_t*(T04 - T5s)
Wt = cp * (T04 - T05)

# 4. Nozzle calculations (non-choked flow)
p6 = pa
T6 = T05 * (p6/p5)**((gamma-1)/gamma)
V6 = m.sqrt(2*cp*(T05 - T6))
M6 = V6/m.sqrt(gamma * R * T6)
```

```
# 5. Performance
V2 = 18  # Inlet velocity
thrust = (ma + mf)*V6 + (p5 - pa)*A6 #- ma*V2
sfc = mf/thrust if thrust > 0 else float('inf')

# Stagnation temperatures
T02 = T2 * (1 + (gamma-1)/2 * (V2/m.sqrt(gamma*R*T2))**2)
T05_real = T05

# === Velocities at key stations ===
V3 = m.sqrt(2 * cp * (T03 - T3))
V5 = m.sqrt(2 * cp * (T05 - T5_exp))  # Usa T5 experimental para
↪  refletir condições reais

M3 = V3 / m.sqrt(gamma * R * T3)
M5 = V5 / m.sqrt(gamma * R * T5_exp)

# ===  Power (kW) ===

Pc = ma * Wc / 1000      # Compressor power in kW
Pt = (ma + mf) * Wt / 1000  # Turbine power in kW


# ===== PRINT ALL RESULTS =====
print("\n=== COMPRESSOR ===")
print(f"Mass flow: {ma:.3f} kg/s")
print(f"Pressure ratio (PR): {PR_comp:.3f}")
print(f"Compression ratio: {(p3/p2)**(1/gamma):.3f}")
print(f"Isentropic efficiency: {eta_c:.2f}")
print(f"Work: {Wc/1000:.2f} kW")
print(f"Outlet stagnation temp (T03): {T03:.2f} K")
print(f"Outlet stagnation pressure (p03): {p03:.2f} Pa")
print(f"Power required: {Pc:.2f} kW")

print("\n=== TURBINE ===")
print(f"Mass flow: {ma + mf:.3f} kg/s")
print(f"Pressure ratio (PR): {PR_turb:.3f}")
print(f"Expansion ratio (ER): {ER_turb:.3f}")
print(f"Isentropic efficiency: {eta_t:.2f}")
print(f"Work: {Wt/1000:.2f} kW")
print(f"Outlet stagnation temp (T05): {T05:.2f} K")
print(f"Power generated: {Pt:.2f} kW")

print("\n=== COMBUSTOR ===")
print(f"Fuel-air ratio: {f:.4f}")
print(f"Combustor outlet temp (T04): {T04:.2f} K")
print(f"Pressure loss: {15:.0f}%")
print(f"Stagnation pressure (p04): {p04:.2f} Pa")

print("\n=== NOZZLE ===")
print(f"Exit velocity: {V6:.2f} m/s")
print(f"Mach number: {M6:.3f}")
print(f"Exit temperature: {T6:.2f} K")
print(f"Area: {A6*1e4:.2f} cm²")
```

```
print("\n=== PERFORMANCE ===")
print(f"Thrust: {thrust:.2f} N (Experimental: 23N)")
print(f"SFC: {sfc*1e6:.2f} mg/N·s")
print(f"Thermal efficiency:
↪  {(thrust*V6)/(mf*fuel_heating_value)*100:.2f}%")
print(f"Total air mass flow: {ma:.4f} kg/s")

print("\n=== KEY RATIOS ===")
print(f"Overall pressure ratio (p3/p2): {PR_comp:.3f}")
print(f"Turbine expansion ratio: {ER_turb:.3f}")
print(f"Compressor temp ratio (T03/T02): {T03/T02:.3f}")
print(f"Turbine temp ratio (T05/T04): {T05/T04:.3f}")
print(f"Fuel-air mass ratio: {1/f:.1f}:1")

print("\n=== VELOCITIES AT STAGES ===")
print(f"Inlet velocity (V2): {V2:.2f} m/s")
print(f"Compressor exit velocity (V3): {V3:.2f} m/s")
print(f"Turbine exit velocity (V5): {V5:.2f} m/s")
print(f"Nozzle exit velocity (V6): {V6:.2f} m/s")
print(f"Mach at compressor exit (M3): {M3:.3f}")
print(f"Mach at turbine exit (M5): {M5:.3f}")
print(f"Mach at nozzle exit (M6): {M6:.3f}")

print("\n=== TEMPERATURES AT EACH STATION ===")
print(f"Ambient temperature (T): {Ta:.2f} K")
print(f"Inlet temperature (T2): {T2:.2f} K")
print(f"Inlet stagnation temp (T2): {T02:.2f} K")
print(f"Compressor outlet temp (T3): {T3:.2f} K")
print(f"Compressor outlet stagnation temp (T3): {T03:.2f} K")
print(f"Combustor outlet stagnation temp (T4): {T04:.2f} K")
print(f"Turbine outlet temp (T5 - experimental): {T5_exp:.2f} K")
print(f"Turbine outlet stagnation temp (T5): {T05:.2f} K")
print(f"Nozzle exit temp (T6): {T6:.2f} K")
```

Listing A.1: Turbojet engine performance calculation

```
# Fuel Efficiency per decade
# Data
decades = ["1970s", "1980s", "1990s", "2000s", "2010s", "2020s"]
efficiency_gain = [25.0, 16.7, 22.7, 15.5, 22.4, 15.8]

# Plot
plt.figure(figsize=(10, 6))
bars = plt.bar(decades, efficiency_gain, color='skyblue',
↪  edgecolor='black')

# Add the labels above the bars
for bar in bars:
    height = bar.get_height()
    plt.annotate(f'{height:.1f}%',
                 xy=(bar.get_x() + bar.get_width() / 2, height),
                 xytext=(0, 5),
                 textcoords="offset points",
                 ha='center', va='bottom', fontsize=10)

# Titles and labels
plt.title("Fuel Efficiency Gain per Decade", fontsize=14)
plt.xlabel("Decade", fontsize=12)
plt.ylabel("Efficiency Gain (%)", fontsize=12)
plt.grid(axis='y', linestyle='--', alpha=0.7)
plt.ylim(0, 30)

# Show and save the graph
plt.tight_layout()
plt.savefig("Fuel_Efficiency_Gain_per_Decade.png")
plt.close()
```

Listing A.2: Fuel efficiency plot generation

```
# Physical congruence
# Data
fuel_injection = np.array([1.94, 2.44, 3, 4, 5, 6, 6.3, 6.44]) # g/s
delta_torque = np.array([0.5721, 0.472, 0.3405, 0.1987, 0.2915,
↪  0.02505, -0.0138, -0.03879]) * 100 # percentage
thrust = np.array([23.8, 25.6,26.8, 28, 29.3, 28.9, 29.9, 28.3]) #
↪  Newton
specific_thrust = thrust / fuel_injection # N.g/s

# Function to plot
def plot_with_interpolation(x, y, y_label, savefig):
    xnew = np.linspace(x.min(), x.max(), 300)
    spline = make_interp_spline(x, y, k=3)
    y_smooth = spline(xnew)

    plt.figure(figsize=(8, 5))
    plt.plot(xnew, y_smooth, label='Interpolation',
    ↪  color='dodgerblue')
    plt.scatter(x, y, color='lime', zorder=5)
    plt.legend(['Interpolation', 'Computional Data'])
    # Add value labels
    for xi, yi in zip(x, y):
        plt.text(xi, yi, f'{yi:.2f}', fontsize=9, ha='center',
        ↪  va='bottom')

    plt.xlabel('Fuel Injection (g/s)')
    plt.ylabel(y_label)
    plt.grid(True)
    plt.tight_layout()
    plt.savefig(savefig)

# Plots
plot_with_interpolation(fuel_injection, delta_torque, 'Delta Torque
↪  (%)', 'delta_torque.png')
plot_with_interpolation(fuel_injection, thrust, 'Thrust
↪  (N)','thrust.png')
plot_with_interpolation(fuel_injection, specific_thrust, 'Specific
↪  Thrust (N.s/g)', 'specific_thrust.png')
```

Listing A.3: Physical congruence plots generation

```
# Other rotations
rpm = np.array([30000, 40000, 50000, 60000])
fuel_injection_rpm = np.array([2.5, 3.5,4.6, 6.2])
thrust_rpm = np.array([8.3, 15.1, 24.3, 29.9])
specific_thrust_rpm = thrust_rpm/fuel_injection_rpm

def plot_with_interpolation(x, y, y_label, savefig):
    xnew = np.linspace(x.min(), x.max(), 300)
    spline = make_interp_spline(x, y, k=3)
    y_smooth = spline(xnew)

    plt.figure(figsize=(8, 5))
    plt.plot(xnew, y_smooth, label='Interpolation',
    ↪  color='dodgerblue')
    plt.scatter(x, y, color='lime', zorder=5)
    plt.legend(['Interpolation', 'Computional Data'])
    # Add value labels
    for xi, yi in zip(x, y):
        plt.text(xi, yi, f'{yi:.2f}', fontsize=9, ha='center',
        ↪  va='bottom')

    plt.xlabel('RPM')
    plt.ylabel(y_label)
    plt.grid(True)
    plt.tight_layout()
    plt.savefig(savefig)

plot_with_interpolation(rpm, thrust_rpm, 'Thrust
↪  (N)','rpm_thrust.png')
plot_with_interpolation(rpm, specific_thrust_rpm, 'Specific Thrust
↪  (N.s/g)', 'rpm_specific_thrust.png')
```

Listing A.4: Rotation analysis code

```
# Efficiency gains
# Data - Turbine
angle = np.array([2, 4, 6, 7, 8])
thrust2 = np.array([29.7, 30.7, 31.7, 32.2, 31.1])
specific_thrust2 = thrust2 / 5


# Data Chamber
percentage_diameter = np.array([1.1, 1.2, 1.3, 1.35])
thrust3 = np.array([33.8,34.1, 34.6, 36.1])
specific_thrust3 = thrust3 / 5

# Function to plot
def plot_with_interpolation_turbine(x, y, y_label, savefig):
    xnew = np.linspace(x.min(), x.max(), 300)
    spline = make_interp_spline(x, y, k=3)
    y_smooth = spline(xnew)

    plt.figure(figsize=(8, 5))
    plt.plot(xnew, y_smooth, label='Interpolation',
    ↪  color='dodgerblue')
    plt.scatter(x, y, color='lime', zorder=5)
    plt.legend(['Interpolation', 'Computional Data'])
    # Add value labels
    for xi, yi in zip(x, y):
        plt.text(xi, yi, f'{yi:.2f}', fontsize=9, ha='center',
        ↪  va='bottom')

    plt.xlabel('Angle (degrees)')
    plt.ylabel(y_label)
    plt.grid(True)
    plt.tight_layout()
    plt.savefig(savefig)


def plot_with_interpolation_chamber(x, y, y_label, savefig):
    xnew = np.linspace(x.min(), x.max(), 300)
    spline = make_interp_spline(x, y, k=3)
    y_smooth = spline(xnew)

    plt.figure(figsize=(8, 5))
    plt.plot(xnew, y_smooth, label='Interpolation',
    ↪  color='dodgerblue')
    plt.scatter(x, y, color='lime', zorder=5)
    plt.legend(['Interpolation', 'Computional Data'])
    # Add value labels
    for xi, yi in zip(x, y):
        plt.text(xi, yi, f'{yi:.2f}', fontsize=9, ha='center',
        ↪  va='bottom')

    plt.xlabel('Percentage of increase of diameter')
    plt.ylabel(y_label)
    plt.grid(True)
    plt.tight_layout()
    plt.savefig(savefig)
```

```
# Plots
plot_with_interpolation_turbine(angle, thrust2, 'Thrust
↪  (N)','angle_thrust.png')
plot_with_interpolation_turbine(angle, specific_thrust2, 'Specific
↪  Thrust (N.s/g)','angle_sthrust.png')
plot_with_interpolation_chamber(percentage_diameter, thrust3,
↪  'Percentage of original diameter (%)','diameter_thrust.png')
plot_with_interpolation_chamber(percentage_diameter,
↪  specific_thrust3, 'Percentage of original diameter
↪  (%)','diameter_sthrust.png')
```

Listing A.5: Efficiency gains analysis code

```
# Cp Turbine

xChord = [
    0.449190974, 0.411827624, 0.382295161, 0.35054031, 0.310484976,
    0.288506359, 0.270561785, 0.22680831, 0.175730228, 0.165727943,
    0.157209352, 0.105650507, 0.0583039895, 0.0525968075,
    ↪  0.0467129201,
    0.0, 0.000323168118, 0.000539674831, 0.0482841842, 0.0555944704,
    0.0628060549, 0.110991538, 0.164070711, 0.173089162, 0.182731673,
    0.23504512, 0.28338185, 0.296682686, 0.311163157, 0.357955664,
    0.399735093, 0.418434262, 0.43909952, 0.477901995, 0.51146692,
    0.536366761, 0.564520597, 0.593497455, 0.617779672, 0.649340272,
    0.685878992, 0.703758299, 0.718265831, 0.756735563, 0.802370727,
    0.808246672, 0.812895179, 0.858334541, 0.901967049, 0.906906903,
    0.912899017, 0.954106927, 0.986046433, 1.0, 0.999523997,
    0.99943167, 0.989765286, 0.960809112, 0.920917749, 0.92057389,
    0.920099437, 0.878568411, 0.846081257, 0.834805369, 0.818893731,
    0.78898555, 0.766124964, 0.74143523, 0.706181288, 0.69186157,
    0.680803835, 0.640232682, 0.588431835, 0.586290658, 0.58332324,
    0.530209064, 0.488712996, 0.471887559
]

Cp = [
    -0.777925789, -0.752855301, -0.734962523, -0.716921508,
    ↪ -0.706068397,
    -0.699370325, -0.732049465, -0.814719498, -1.07239974,
    ↪ -1.12483144,
    -1.1856184, -1.54787469, -1.75729764, -1.78413498, -1.70236075,
    -0.942584574, -0.008857999, 0.569824994, 0.893859625,
    ↪  0.943405867,
    0.930005133, 0.817794621, 0.677734017, 0.650797248, 0.619593084,
    0.445805639, 0.377005845, 0.358031273, 0.350920737, 0.327757925,
    0.307366371, 0.297115386, 0.283544332, 0.257532895, 0.226512864,
    0.20250392, 0.174292013, 0.145701692, 0.120885305, 0.0879778489,
    0.0471975468, 0.0271448269, 0.00910566561, -0.0392528735,
    ↪ -0.10106276,
    -0.109082006, -0.115963273, -0.183354408, -0.255484343,
    ↪ -0.26367116,
    -0.274190098, -0.34760347, -0.497906804, -0.563337803,
    ↪ -0.682385385,
    -0.704186499, -0.707556248, -0.716152728, -0.743903399,
    ↪ -0.744150162,
    -0.744571805, -0.783647001, -0.811061561, -0.821958899,
    ↪ -0.833964765,
    -0.859499335, -0.870820165, -0.882533252, -0.884134293,
    ↪ -0.885572433,
    -0.883978724, -0.879960835, -0.8630265, -0.862403154,
    ↪ -0.860936522,
    -0.835932314, -0.805078924, -0.793434918
]
```

```
plt.figure(figsize=(8, 5))
plt.plot(xChord, Cp, color='dodgerblue')
plt.scatter(xChord, Cp, color='lime', zorder=5)
plt.xlabel('Chord Length')
plt.ylabel('Pressure coefficient')
plt.grid()
plt.gca().invert_yaxis()
plt.savefig('cp_turbine.png')
plt.close()
```

Listing A.6: Turbine pressure coefficient analysis